Impact of storm propagation speed on coastal flood hazard induced by offshore storms in the North Sea

Xiaoyan Wei[1], Jennifer M. Brown[1], Joanne Williams[1], Peter D. Thorne[1], Megan E. Williams[1,2], Laurent O. Amoudry[1]

[1]National Oceanography Centre, Joseph Proudman Building, 6 Brownlow Street, Liverpool L3 5DA, United Kingdom.

[2]Departamento de Obras Civiles, Universidad Técnica Federico Santa María, Avenida España 1680, Valparaíso, Chile.

Corresponding author: Xiaoyan Wei (xwei@noc.ac.uk)

Key words:

storm propagation speed; tide-surge interaction; extreme water level; resonance; wind set-up; North Sea

Abstract

Storm propagation speed (SPS) can noticeably impact coastal floods around semi-closed basins influenced by extratropical offshore storms. As a case study, the SPS impact on potential flood hazards due to extreme water levels along the UK east coast was studied using a numerical shelf sea model (FVCOM). The storm Xaver, which caused the largest North Sea surge over the past 60 years, was studied as a base scenario. Halving/doubling the SPS results in a smaller surge and a longer/shorter surge duration. Hence, the largest peak water level was found at actual speed, while the largest potential flood hazard occurred at half speed. Tide-surge interaction tends to reduce the M2 tide along the coast and advance its propagation for all SPS. A three-dimensional semi-analytical model, including a time-periodic wind forcing, was used to investigate the dominant mechanisms behind the surge dynamics, where wind duration is directly related to the SPS. Long wind durations correspond to small SPS, and vice versa. The semi-analytical model was applied to the North Sea. The model reproduces the spatial features of the North Sea surge and its dependence on SPS, confirming the surge induced by offshore storms is primarily associated with wind set-up. Model results suggest the SPS of Xaver is likely to have contributed greatly to the occurrence of the largest North Sea surge due to wind-generated resonance. The impact of the SPS on the surge and tide-surge interaction are of great importance to coastal flood hazard assessment.

Plain Language Summary

Coastal floods are among the most devastating natural hazards in coastal regions. The present study investigates the impact of the storm speed on coastal flood hazards at locations hundreds of kilometres away from the maximum winds. We focused on a case study for the east coast of the United Kingdom during the storm Xaver (5-6 December 2013), which caused the largest surge height in the North Sea over the past 60 years. Our results show the storm-induced flood hazard varies significantly with distance from the storm track and poses a great threat to the southeast coast of the UK. The largest flood hazard was found when the storm moves slowly, but the largest water level occurred when the storm travels at the actual speed of Xaver. The rise of water level due to wind (i.e., wind set-up) is the main contributor to the storm surge in the study site, and is strongly dependent on the water depth, fetch length and the wind duration. The UK southeast coast having a longer fetch and fronted by shallow waters with a low tidal range is the most vulnerable area in terms of coastal flooding due to large storm surge. The storm and tide can interact with each other and decreases the maximum water level, thus reducing the potential flood hazard especially at coasts with a large tidal range. Significant rises of water level can be generated by wind set-up when the dominant wind frequency (related to the storm speed) is close to the resonant frequency of the basin. Our results show that storm speed is an important factor for coastal flood hazard assessment.

1 Introduction

Floods due to storm-induced ocean surges are among the most devastating natural disasters in coastal areas. Hurricane Katrina (August 2005) was one of the costliest and deadliest natural disasters recorded in the US. It caused damages estimated at $158.2 billion (Cavallo & Noy, 2010) and over 1500 deaths (Kates et al., 2006), most of which were related to coastal flooding. In the North Sea, the devastating 1953 storm (January-February 1953) caused widespread and persistent flooding, resulting in an estimated damage of $7 billion adjusted for inflation (Risk Management Solutions, 2003) and over 2000 deaths (Jonkman & Kelman, 2005). This storm directly led to the construction of most coastal sea defences around the North Sea and greatly changed coastal management.

Coastal floods are significantly influenced by storm characteristics such as storm track, intensity and size (Azam et al., 2004; Benavente et al., 2006; Brown et al., 2010; Haigh et al., 2016; Hussain et al., 2017; Irish et al., 2008; Peng et al., 2004; Rego & Li, 2009; Souza et al., 2013). The storm propagation speed (SPS) can also be crucial for storm surge generation and the consequent flooding (Hussain et al., 2017; Irish et al., 2008; Jelesnianski, 1972; Maskell, 2011; Peng et al., 2004; Peng et al., 2006; Rego & Li, 2009; Weisberg & Zheng, 2006; Zhang, 2012; Bertin et al., 2012). Focusing on hurricanes that make landfall or in close proximity to the coastline at a specific site of interest, Peng et al. (2004) found that slower SPS resulted in larger peak surge heights and inundation area in the eastern North Carolina, USA. Similar findings exist for the central Florida coast (Weisberg & Zheng, 2006) and for an idealized shelf (Irish et al., 2008). However, Rego and Li (2009) found an opposite trend over the Louisiana-Texas shelf, where slower SPS resulted in smaller peak surge heights. The different impacts of SPS on storm surge may be related to the different distances from the storm track, as suggested by Peng et al. (2006) and Hussain et al. (2017). The latter found that, in the Bay of Bengal (Bangladesh), decreasing SPS led to smaller surge heights at locations within the radius of maximum wind and a stronger surge at locations outside the radius. Moreover, they found the arrival time of the maximum surge residual (total water level subtracted by astronomical tide) was more affected by tidal phases for slower SPS, and maximum surge residual always occurred near high tides for slowly propagating storms. Storm propagation speed can also greatly influence the storm surge through resonance effects. Extremely large oscillations can occur when the SPS is close to the phase speed of the ocean water wave, i.e., Proudman resonance (Proudman 1929). Strong oscillations can also be generated when the atmospherically generated ocean wave has periods equal to the eigen (resonance) period of the shelf region, i.e., shelf resonance (Monserrat et al., 2006; Bertin et al., 2012). Hence, SPS can be crucial for causing severe coastal flood hazard when the associated wind period (here assumed to be twice the duration of winds capable of generating a positive surge during the storm) is close to the eigen period of the coastal basin. These findings suggest that SPS can have a significant impact on coastal flood hazard through affecting the storm surge and tide-surge interaction, with its impact depending on the distance from the storm track.

As indicated above, most previous studies on SPS have focused on tropical cyclones and their impact on coasts directly under or within close proximity to the storm track during the storm landfalls. The impact of SPS on coastal flood hazard where the storm track remains distant from the site(s) of impact has not been as well studied. In reality, there can be a large storm surge generated flood hazard even under distant storm conditions. Tropical cyclones can induce significant water level rises at the coast ahead of the storm landfall, i.e., forerunner surges (Kennedy et al., 2011; Liu & Irish 2019), causing large coastal flood potentials. Extratropical storms, which generally move faster than tropical cyclones and have not been as well studied in terms of the SPS effect, can also greatly affect sites distant from the storm track. The east coast of the UK, for example, has been frequently flooded by storm surge events even though the storms usually track parallel to the coastline at some distance offshore or easterly along the open northern boundary of the North Sea (Haigh et al., 2016). Focusing on extratropical storms, the present study aims to improve understanding of the SPS impact on coastal flood hazards due to extreme water levels at locations distant from the storm track. The impact of SPS on tide-surge interaction, which was not accounted for in many previous studies (e.g., Peng et al., 2004, 2006; Weisberg & Zheng, 2006), is also investigated here due to its importance for accurate storm surge forecasting in macro-meso tidal environments.

To evaluate the impact of SPS at locations distant from the storm track and to investigate the underlying physical mechanisms, the UK east coast has been selected as a case study. The tidal range along the UK east coast is mostly above 2 m (meso- and macro-tidal) with the largest tidal range of ~6 m near Immingham. Water depths of less than 10 m extend several kilometers from the southeast coast of the UK, leading to strong tide-surge interactions in this area. Tides are known to have a strong impact on the arrival time of the maximum surge residual in the North Sea (Prandle & Wolf, 1978; Wolf, 1978). Statistical analysis of Horsburgh & Wilson (2007) shows that, along the

UK east coast, maximum surge residual tends to occur 3-5 hours before the next high water, and the likelihood of the maximum surge residual occurring near high water decreases with increasing tidal range. The largest storm surge in the North Sea over the past 60 years, named 'Xaver' by the Free University of Berlin, occurred during the storm event on 5-6 December 2013 (Harwood, 2013). This storm had a similar (although less southerly) track and intensity, with similar alongshore wind, down the UK east coast, to the previously-mentioned 1953 storm, when the storm centre travelled across the North Sea. However, the 2013 storm propagated about twice as fast (Wadey et al., 2015; Sibley et al., 2015) as the 1953 storm. The 2013 storm also coincided with larger astronomical tides, while the 1953 event had a larger onshore wind component, which resulted in a larger significant wave height along the English east coast. The 2013 event caused coastal flooding along the UK east coast, with the overall damage (around $900 million, see Rucińska (2019)) much less severe than for the 1953 event. The limited damage has been mostly attributed to significant improvement in sea defences (Swaden et al., 2014), but we show here that the faster SPS also played a significant role. In this study, the impact of SPS on storm surge and its consequent coastal flood hazard due to extreme water levels were investigated using a numerical shelf sea model, which includes state-of-the-art parameterizations and physical processes. This model was also used to examine the impact of SPS on tides through tide-surge interaction. An idealized semi-analytical surge model was also used to investigate the dominant physical mechanisms behind the impact of SPS.

The paper is structured as follows: in section 2, the numerical shelf sea model set-up (section 2.1), the numerical experiments (section 2.2), and the details of the semi-analytical model (section 2.3) are introduced. In section 3, the impacts of SPS on coastal flood hazard due to extreme water levels are quantified, with the influence of SPS on extreme water levels, surge and tide-surge interaction, and its impact on tides discussed in section 3.1, section 3.2 and section 3.3, respectively. In section 4, the physical mechanisms governing the surge dynamics are explored. In section 4.1, the relative contribution of air-pressure gradients and wind stress to storm surge is investigated. In section 4.2, the sensitivity of surge to water depth and fetch length is examined based on the semi-analytical model. In section 4.3, the semi-analytical model is applied to the North Sea, where the sensitivity of surge to wind duration is explored. Conclusions are drawn in section 5.

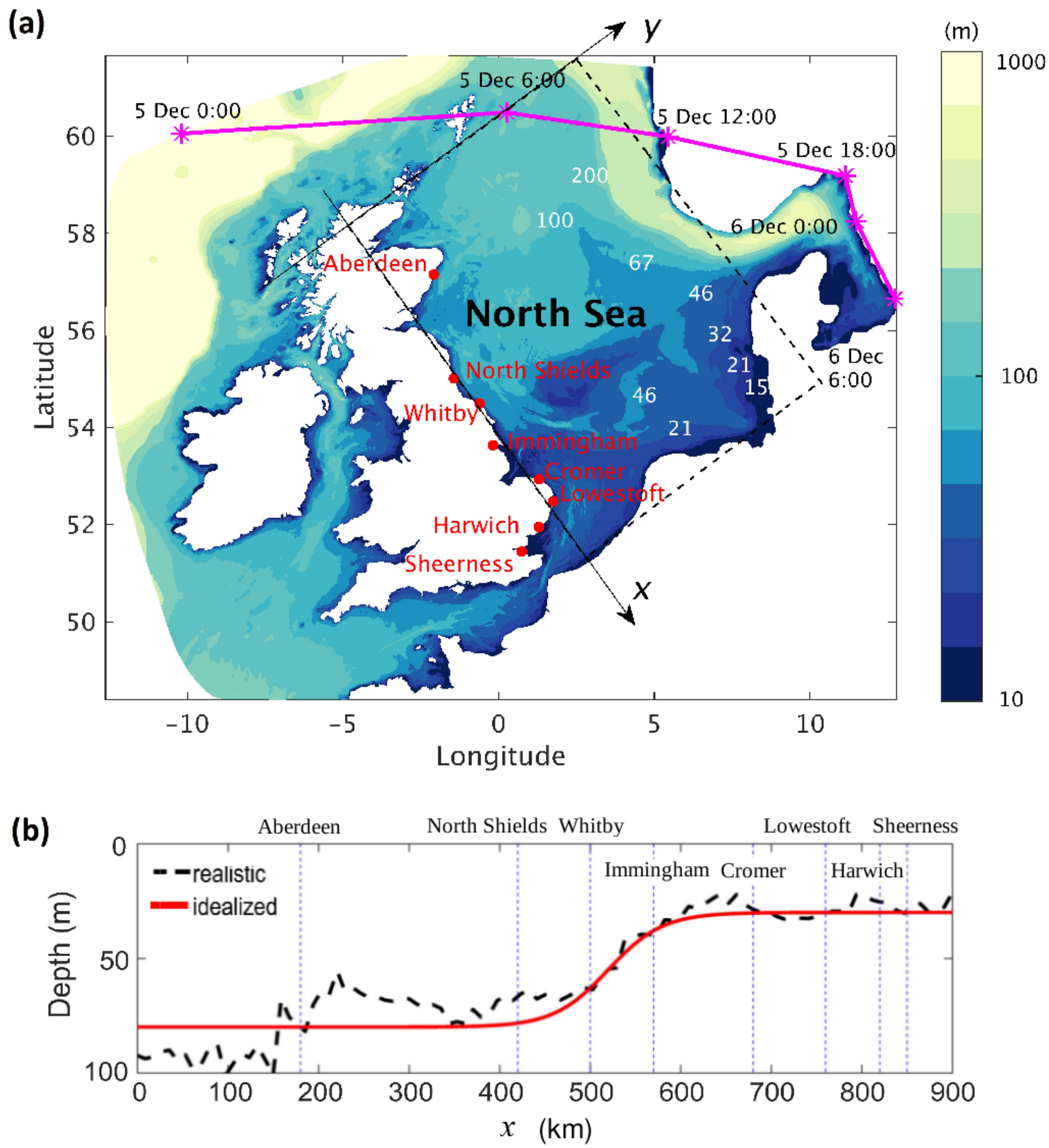

Figure 1. (a) The bathymetry in the FVCOM model domain. The pink line indicates the storm track of Xaver, with the centre of the storm (position of the lowest atmospheric pressure) at every 6 hours marked by asterisks. The red dots represent the eight UK east coast tide gauge stations. The dashed rectangle shows the idealized geometry of the North Sea discussed in section 2.3. (b) The width-averaged real and idealized depth of the North Sea, with x the along-coast coordinate positive southward.

2 Methods

2.1 The FVCOM model

To quantify the impact of SPS on the coastal flood hazard due to extreme water level along the UK east coast, a shelf sea model (Wolf et al., 2016), which is based on the finite-volume community ocean model (FVCOM, see Chen et al. 2003), was used. The study focuses on the UK east coast, but the model includes the entire North West European Shelf and extends beyond the shelf break (see Figure 1a) to reduce the effect of boundary errors on solutions within the area of interest. i.e., the UK east coast. Complex coastal geometries and bathymetries are captured by using an unstructured grid. The mesh resolution varies from ~30 km at the open boundary to ~1 km at the coast. The model uses 20 vertical sigma layers.

The base scenario of this study is the storm event Xaver on 5-6 December 2013, of which the storm track is shown by the pink line with asterisks giving the location every 6 hours in Figure 1a. As this work focuses on the storm-induced coastal flood hazard, the model was run in barotropic mode which resolves tide, surge and tide-surge interaction. Dynamic influences of short waves are excluded in the model due to their small impact in the 1953 and 2013 events, in which they increased the peak surge by less than 0.25 m (10%) in most areas of the North Sea (Staneva et al., 2017 and Choi et al., 2018). The forcing conditions include tidal elevations at the offshore boundary, and wind and atmospheric pressure at the free surface. At the open boundary, the water levels were provided by the tide-only runs of the UK operational surge model CS3X (Flather 1994), which takes into account the astronomical tidal potential forcing. Effects of local tide potential force were ignored since the North Sea is relatively shallow. The surface air pressure and wind velocities (at 10 m above surface) were obtained from the hourly output of the Met Office deterministic Global model (Davies et al., 2005), which were linearly interpolated into each time step within the FVCOM model. The accuracy of the wind forcing obtained from the Met Office deterministic Global model is checked by comparing the wind forcing datasets at eight wind stations close to the UK east coast with wind observations throughout the storm Xaver (for details, see Figure A.3 and Table A.1 in the appendix). The mean error and the root-mean-squared error of the wind speed averaged over the eight wind stations are respectively 3.88 m/s and 6.00 m/s. The meteorological forcings at every 6 hours during the storm Xaver are shown in Figure 2. The storm travelled across the North Sea from west to east, and the centre of the storm (i.e., position of the lowest atmospheric pressure) remained distant from most of the UK coast. The prevailing wind was into the North Sea (i.e. northwest wind). The maximum wind velocity at the northern end of the North Sea during the storm event was around 20 m/s, which decreased southward along the coast. The simulation period is 4 December 2013 17:00 to 12 December 2013 17:00, covering short periods of pre- and post-storm. The model was spun up from 1 November 2013 00:00 to 4 December 2013 17:00.

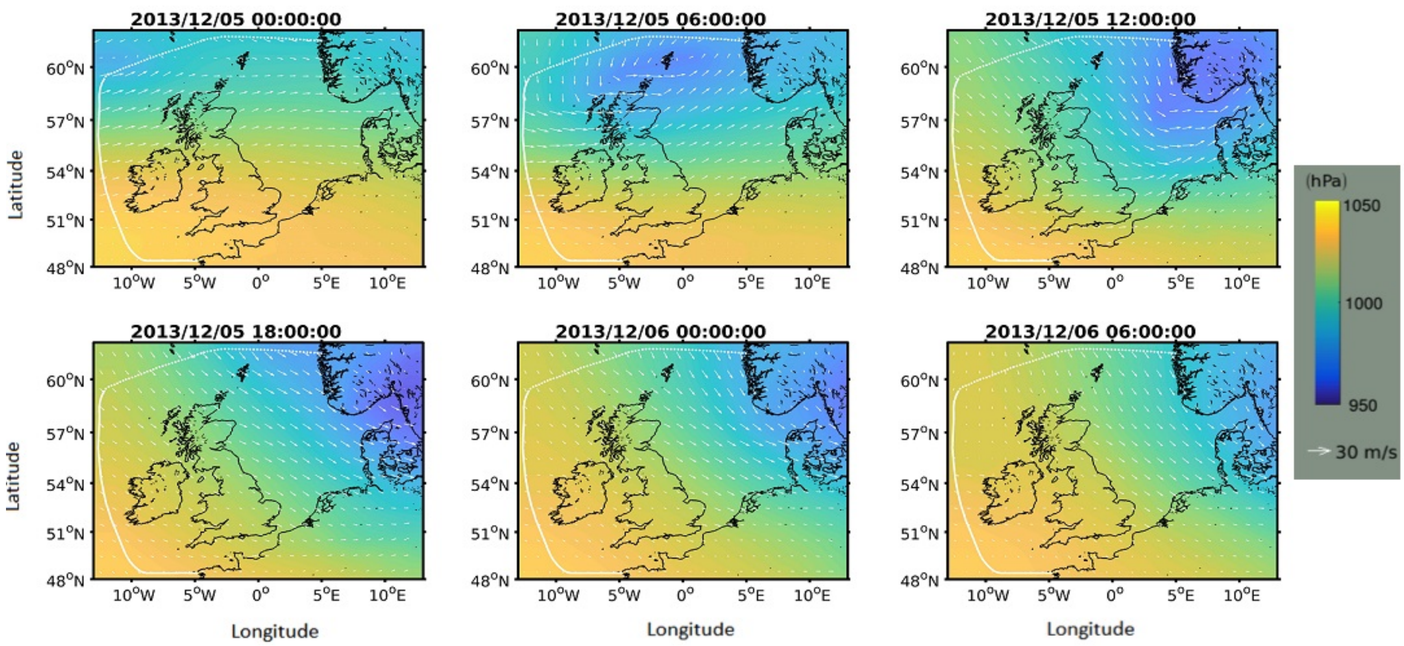

Figure 2. Meteorological forcings at every 6 hours during Xaver. Wind velocities and atmospheric pressure are shown in white arrows and colours, respectively. The bluest area represents the lowest atmospheric pressure. The white dotted line shows the open boundary of the FVCOM model.

In the FVCOM model, the wind stress is calculated based on wind velocities (u_w, v_w) and the surface drag coefficient C_d, $(\tau_{wx}, \tau_{wy}) = \rho_{air} C_d (u_w, v_w)\sqrt{u_w^2 + v_w^2}$, with ρ_{air} the air density. The default surface drag formula in FVCOM follows the formula of Large and Pond (1981) but resulted in under-predicted surge conditions at the study site. To improve the model performance throughout Xaver, an improved parameterization was used and the surface drag C_d is related to the surface wind stress using a Charnock parameterization (Charnock, 1955; Brown and Wolf, 2009). Focusing on the German Bight, Zheng et al. (2018) found the wind drag coefficient during Xaver to vary approximately linearly with the wind speed for relatively deep waters. Since most of the North Sea is deeper than the German Bight, the Charnock parameterization of the surface drag was fitted into a linear function of the wind speed (U_{wind}):

$$C_d = C_1 + C_2 U_{wind}. \tag{1}$$

Here C_1 and C_2 are two wind drag coefficients, which, together with the seabed roughness length scale z_0, were tuned to obtain the best fit of water levels in comparison with observations. The model performance was assessed by comparing the simulated water levels against observations at eight tide gauges along the UK east coast. Tuning the wind drag coefficients partly accounts for the short wave impact on storm surge through the enhanced roughness. But, the other processes related to short waves and wave-current interactions are not considered here due to the negligible wave setup in the domain of interest during Xaver (Staneva et al., 2017).

Table 1. Skew surge and mean tidal range at each station. Mean error (*ME*), root-mean-squared error (*RMSE*), Willmott index of agreement (*d*) for the total water level.

Gauge station	Skew surge[a]		Tidal range[b]		Total water level		
	observed (m)	simulated (m)	observed (m)	simulated (m)	*ME* (m)	*RMSE* (m)	*d*
Aberdeen	0.64	0.67	3.67	3.87	0.05	0.15	0.9954
North Shields	1.18	1.09	4.06	4.67	0.07	0.17	0.9962
Whitby	1.47	1.28	4.52	4.81	-0.11	0.19	0.9957
Immingham[c]	1.52	1.49	-	6.8	0	0.2	0.9933
Cromer	1.22	1.75	3.63	4.24	0.17	0.28	0.9895
Lowestoft	2.06	1.96	1.67	2.11	0.11	0.16	0.9904
Harwich	1.3	1.4	3.58	3.69	-0.39	0.21	0.9918
Sheerness	1	1.45	5.14	4.74	-0.23	0.68	0.9527
Average	1.3	1.38	-	4.36	-0.01	0.26	0.9900

Note:

[a] The skew surge was calculated for the stormy period: 5 December 2013 00:00 to 6 December 2013 19:00.

[b] The mean tidal range was calculated for the non-stormy period by averaging the tidal ranges of all tidal cycles from 6 December 2013 19:00 to 8 December 2013 21:00.

[c] The tide gauge at Immingham was damaged on 06 December 2013 at 17:00, so the *ME, RMSE* and *d* at this station were calculated based on data from 4 December 2013 17:00 to 6 December 2013 17:00.

By calibrating the model against observed water levels, $C_1 = 0.81\times10^{-3}$, $C_2 = 0.09\times10^{-3}$ s/m and $z_0 = 0.0035$ m were found to give the best fit. Details of the model performance at each gauge station are summarized in Table 1, including the skew surge, mean tidal range and the total water level. The total water level is the water level under effects of tide, surge and their interactions, and skew surge is the difference between the maximum total water level and the peak astronomical tidal elevation during the storm. The simulated/observed skew surge and mean tidal range calculated respectively for the stormy period and non-stormy period show the model reproduces the surge and tidal magnitudes reasonably well during the storm event. For the predicted and observed total water levels the mean error (*ME*) and the root mean squared error (*RMSE*) averaged over all gauges (marked by red dots in Figure 1a) are -0.01 m and 0.26 m, respectively, both of which are small relative to the mean tidal range (4.36 m) and mean skew surge (1.38 m). We also report the index of agreement following Willmott (1981), $d = 1 - \sum_{i=1}^{N}(P_i - O_i)^2 / \sum_{i=1}^{N}(|P_i - \bar{O}| + |O_i - \bar{O}|)^2$, which measures the skill of the model with $d = 1$ for perfect agreement and $d = 0$ for complete disagreement. P_i and O_i are respectively model predictions and observations, and the overbar denotes the mean value. Table 1 shows that, for all stations, *d* is close to 1 with an averaged value of over all 8 stations of 0.9900, slightly larger than that of the CS3X model (0.9762), confirming the FVCOM model is accurate enough for this study. Figure 3 shows the time series of simulated water levels from the FVCOM model (red lines) and the UK operational CS3X model (blue lines), in comparison with observations (black circles). At all stations except Cromer, the FVCOM model reproduces the storm event better, whereas the CS3X model (spatial resolution approximately 12 km) underpredicts the peak water level at all locations. The largest discrepancy between the FVCOM model results and observations occurs at Sheerness, where the FVCOM model overpredicts the low water and the tidal phase especially during falling tides, hence yielding a large *RMSE*. This could be related to the fact that the resolution of 1 km at the coast is insufficient to capture the bathymetric variations inside the Thames Estuary where the water depth changes dramatically from thalweg to shoals over short distances. As this study focuses on the UK east coast, the impact of mesh resolution on the accuracy of storm surge hindcast inside the Thames estuary is not further explored here.

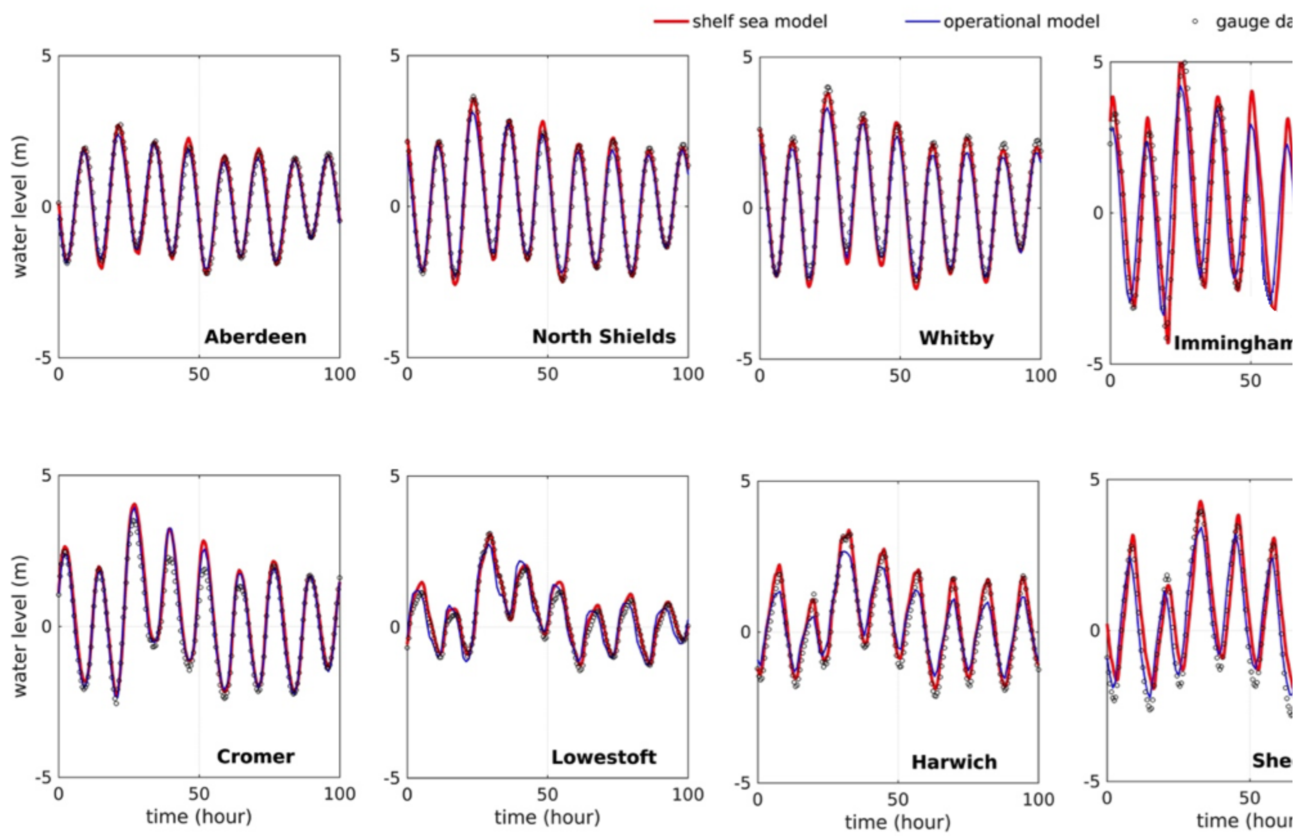

Figure 3. Water level relative to mean sea level simulated by the (FVCOM) shelf sea model (red lines) and the UK operational CS3X model (blue lines) in comparison with gauge data (black circles). The time period shown here is from 4 December 17:00 to 8 December 21:00 in 2013. The gauge data at Immingham after 17:00 pm, 06 December 2013, is not available due to damaged tidal gauge.

2.2 Numerical experiments design

Nine numerical experiments were designed to study the influence of SPS on extreme water levels along the UK east coast. The parameter settings for each experiment are summarized in Table 2. In experiment I, the actual Xaver event was modeled and used to calibrate the model. In experiments II and III, the propagation speed of Xaver was doubled and halved, respectively. This was realized by respectively halving and doubling the time intervals of the wind and atmosphere pressure time series, while keeping other conditions and parameters the same as in experiment I. The dynamic impact of SPS on the storm intensity, track and wind field asymmetry, which can be significant for tropical cyclones especially near the storm centre (see, e.g, Mei et al., 2012 and Olfateh et al. 2017), are neglected here. This is because impact of SPS on extratropical cyclones is not well understood and the numerical experiments in this study were designed to isolate the impact of SPS. Experiment III is representative of the 1953 storm, although other differences between two events (such as the storm track) are excluded so that the impact of SPS can be isolated. In experiment IV, both atmospheric pressure gradients and wind were prescribed to be zero, therefore modelling the astronomical tidal elevations. In experiments V, VI and VII, tidal forcing was excluded, and the model was forced by the meteorological forcing with actual, doubled and halved SPS, respectively. These three experiments were taken as the surge-only case for each SPS. Experiments VIII and IX were designed to investigate the relative importance of atmospheric pressure and wind upon the storm surge, where atmospheric pressure gradients and wind stresses were respectively prescribed to be zero.

Table 2. Parameter settings for each numerical experiment. Superscripts d, a and h respectively represent double, actual, and half speed. The subscript TS indicates both tide and surge, T denotes tide only, and S signifies surge only. Subscripts Sw and Sa respectively represent surge induced by wind only and atmospheric pressure only.

Case	Water level	Tide	Storm propagation speed (SPS)	Atmospheric pressure gradient		Wind stress	
				Magnitude	Time interval	Magnitude	Time interval
I	η_{TS}^{a}	actual	actual	actual	actual	actual	actual
II	η_{TS}^{d}	actual	double	actual	half	actual	half
III	η_{TS}^{h}	actual	half	actual	double	actual	double
IV	η_{T}	actual	-	0	-	0	-
V	η_{S}^{a}	0	actual	actual	actual	actual	actual
VI	η_{S}^{d}	0	double	actual	half	actual	half

VII	η_S^h	0	half	actual	double	actual	double
VIII	η_{Sw}^a	actual	actual	0	-	actual	actual
IX	η_{Sa}^a	actual	actual	actual	actual	0	-

2.3 Semi-analytical model

The FVCOM model provides an overall picture of the realistic storm surge in the North Sea during Xaver, however, it is computationally costly and time consuming for isolating contributions from different physical processes through repeated reduced-physics simulations, hence FVCOM is inefficient for sensitivity studies.

Therefore, to investigate the dominant physical mechanisms behind the impact of SPS on surge induced by offshore storms, a three-dimensional semi-analytical model was set up which considered a semi-enclosed rectangular basin with a uniform width. This model solves the linearized three-dimensional shallow water equations on the *f*-plane (constant Coriolis coefficient), assuming hydrostatic equilibrium and negligible lateral bathymetric variations, tidal advection, and baroclinic effects. The bottom friction was introduced by applying a partial slip boundary condition at the seabed: $A_v\,(\partial u/\partial z, \partial v/\partial z) = s(u, v)$, with s the partial slip parameter and A_v the vertical eddy viscosity (Wei et al., 2017). This model was forced by a time-periodic surface stress due to winds blowing along the basin with negligible spatial differences, as well as a time-periodic surge prescribed at the northern end of the basin. More details about this model can be found in the appendix. By considering a periodic wind forcing and surge response, the time evolution of the surge can be calculated by only computing the surge amplitude, without requiring numerical simulations for each time step. As such, the computational cost of the semi-analytical model is significantly reduced compared with the FVCOM model, making it a useful tool for sensitivity studies. The semi-analytical model also provides insights into the physical mechanisms behind the storm surge, which are useful for the interpretation of the numerical results from any surge forecast/hindcast model.

For any along-coast varying depth and wind stress profile with non-negligible bottom friction and Coriolis effect, a semi-analytical method can be used to calculate the surge following the same procedures as Chen et al. (2016), details of which are in the appendix. Due to the low computational cost of this semi-analytical method, the sensitivity of η_{Sw} to SPS can be systematically investigated. Here, SPS is related to the wind duration, which is another important parameter for storm surge apart from the wind speed and direction (Ganske et al., 2018).

For a constant water depth H and spatially uniform time-periodic wind stress along the basin, with negligible Coriolis effect ($f = 0$) and bottom friction ($s = 0$), the surge (η_{Sw}) can be solved analytically following Chen (2015), see appendix for details. The solution is:

$$\eta_{Sw} = \left[\frac{a_w \cos(\gamma(x-L))}{\cos(\gamma L)} + \frac{\hat{\tau}_{wx}\sin(\gamma x)}{\rho g H \gamma \cos(\gamma L)}\right] \sin(\omega t)\,, \text{with } \gamma = \frac{\omega}{\sqrt{gH}}. \qquad (2)$$

Here a_w is the surge amplitude prescribed at the northern boundary; $\hat{\tau}_{wx}$ is the amplitude of the along-coast wind stress; x is the along-coast coordinate (with $x = 0$ at the northern boundary and $x = L$ at the southern boundary); g denotes the gravitational acceleration, ρ the water density, L the basin length and t the time. The wind frequency is denoted by $\omega = \frac{2\pi}{T}$, with T the wind duration (period) assumed to be equal to the surge duration. Equation (2) suggests that the storm surge in the North Sea is influenced by a remotely generated wave through the surge forcing at the northern boundary (first term), and a locally generated wind set-up due to wind stress at the free surface (second term).

To qualitatively represent the geometric and bathymetric features of the North Sea, the basin width and length are approximated to be 500 km and 900 km, respectively, and the depth is allowed to vary along the coast, as described by

$$H = \frac{H_{south}+H_{north}}{2} + \frac{H_{south}-H_{north}}{2} \tanh\left(\frac{x-x_s}{L_s}\right), \qquad (3)$$

with $x_s = 520$ km and $L_s = 60$ km. Equation (3) results in a constant water depth in the north (H_{north}=80 m) and south (H_{south}=30 m), connected by a sharp depth change around Immingham (see Figure 1b). To qualitatively capture the spatial variation of the wind field during Xaver (see Figure 2), the lateral wind stress was taken to be zero; the amplitude of the along-coast wind stress $\hat{\tau}_{wx}$ was fitted to a linear function of x using the width-averaged wind forcing within 200 km off the UK east coast:

$$\hat{\tau}_{wx} = \hat{\tau}_m(1 - 0.74x/L)\,. \qquad (4)$$

Here $\hat{\tau}_m = 2.54$ Pa is the wind stress at the North end $x = 0$. The Coriolis coefficient was taken to be constant, $f = 1.18\times10^{-4}$ rad/s (latitude at ~54° N, *f*-plane approximation).

As a first step to validate the semi-analytical model given by equations A.1-A.5, the semi-analytical model results were compared with the analytical solution (2), considering a constant water depth and along-coast wind stress with $f = 0$ and $s = 0$. The semi-analytical model gives the same results as the analytical solution (see Figure A.1 in the appendix). Then, the semi-analytical model was calibrated with the peak surge (i.e., maximum η_S) obtained from the FVCOM model by tuning a_w, s and A_v. By using a parameter set of $a_w = 0.3$ m, $s = 0.0015$ m/s, and $A_v = 0.016\,\mathrm{m}^2/s$, the spatial distributions of the peak surge distributions of the North Sea obtained from the FVCOM model are qualitatively reproduced for each speed (see Figure A.2 in the appendix and more discussion in section 4.3). This indicates that the simplified geometry, bathymetry and boundary conditions used in the semi-analytical model are appropriate, and the dominant physical processes governing the storm surge are reasonably resolved.

3 Quantifying the impacts of SPS on coastal flood hazard due to extreme water level

Coastal flood hazard is strongly related to the magnitude and duration of extreme water level. To quantify the significance of SPS on coastal flood hazard due to extreme water level along the UK east coast, the FVCOM model described in section 2.1 was used to simulate the tide, surge and their interactions for Xaver at actual (I), double (II) and half (III) SPS. The impact of SPS on coastal flood hazard due to extreme water level is evaluated by comparing the total water level induced by both tide and surge (denoted as η_{TS}), skew surge, and time integrated excess elevation (defined as the time integration of the water level exceeding MHWS, see Lyddon et al. (2018)). Skew surge is a measure of the maximum water level residual induced by the storm, and the time integrated excess elevation is used here as a proxy of potential flood hazard due to limited sea defence freeboard and changing storm duration. Since the extreme water level is a result of the combination of tide, surge, and their interactions, the impact of SPS on surge, tide-surge interaction, and its impact on tides were also investigated.

3.1 Influence of SPS on coastal flood hazard

For these storms, the total water level η_{TS} variations with changing SPS are largest at the southern locations Cromer, Lowestoft, Harwich and Sheerness (Figure 4a). At all stations, the largest η_{TS} was found at actual speed. However, the duration and the number of occurrences of the total water level exceeding MHWS (i.e., high water events) are largest at half speed especially at the southern stations. Figure 4a also shows that, for smaller SPS, high water events occur at a later time, which allows for a longer lead time for flood warning, but also take longer to recede and hence have a larger potential to cause severe flood hazards.

To evaluate the influence of SPS on coastal flood hazard due to extreme water levels, the skew surge and time integrated excess elevation were calculated (Figure 4b). When the SPS is equal to the actual speed of Xaver, the largest flood hazard occurs at Lowestoft, with both skew surge and time integrated excess elevation increasing southward from Aberdeen to Lowestoft and decreasing further southward (red lines). Halving the SPS results in a smaller skew surge at all stations, however, the spatially (north-south) varying pattern remains almost unchanged (blue line with circles). Doubling the SPS also results in a smaller skew surge, which constantly increases southward (black line with circles). At stations north of Lowestoft, the skew surge is larger at half speed than that at double speed, but is the opposite at locations south of Lowestoft. This trend change is related to the different arrival time of peak surge with respect to the tide at different locations. North of Lowestoft, the surge in both half- and double-speed cases peaks close to low water (see Figure 5c), but the surge elevation at the next high water in the half-speed case is larger due to the longer storm duration. South of Lowestoft, the peak surge for the double- and half-speed storms is similar, but occurs closer to high water in the double-speed case.

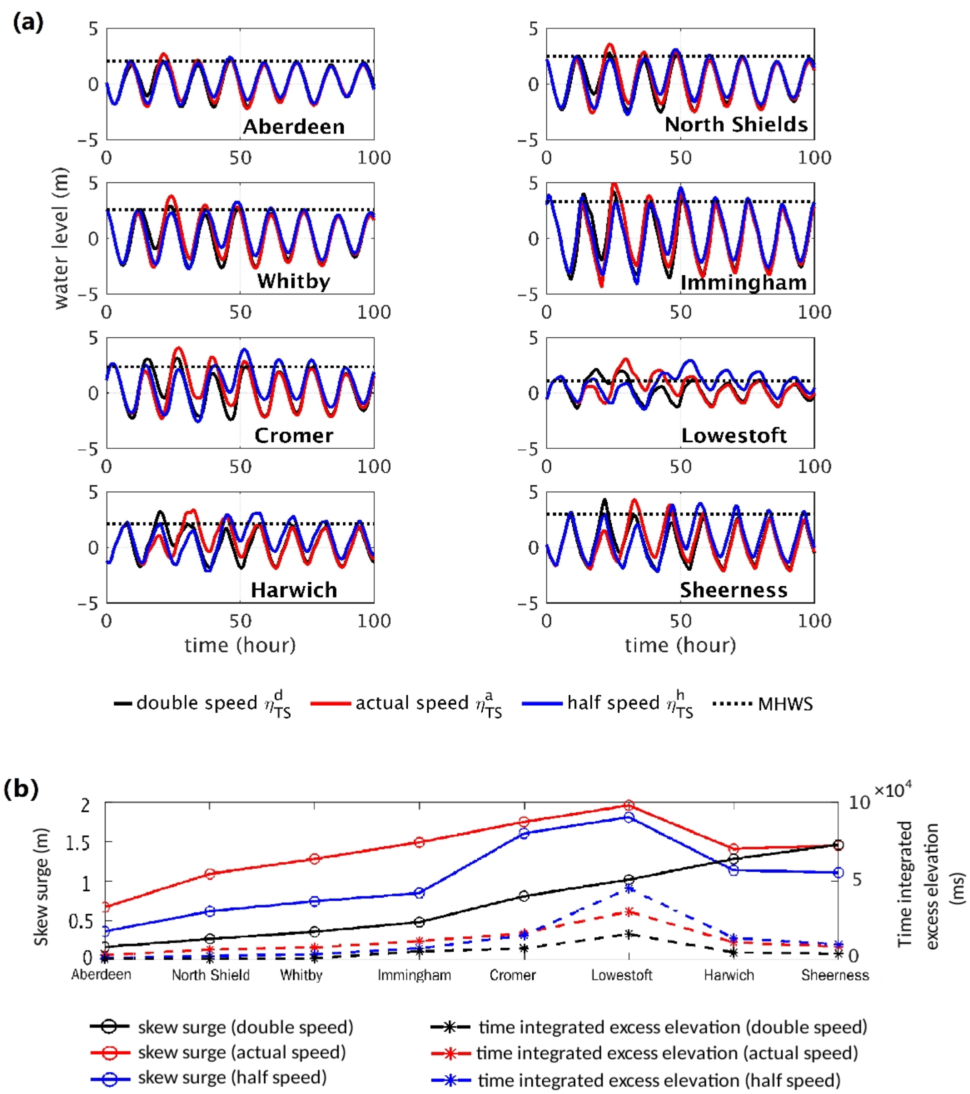

Figure 4. (a) The total water level relative to mean sea level, (b) skew surge and time integrated excess elevation at different stations during the storm event. Red, black and blue lines show results for actual, double and half SPS, respectively. Plots were made using the FVCOM model results

from 4 December 17:00 to 8 December 21:00 in 2013, where the black dotted lines show the mean high water springs.

The spatial trend of the time integrated excess elevation does not change with SPS, with the maximum occurring at Lowestoft for all SPS. Doubling the SPS results in a smaller time integrated excess elevation at all stations (see red and black lines with stars). Halving the SPS results in smaller time integrated excess elevations at the north-eastern stations (Aberdeen to Immingham), and larger excess elevations at the southern stations (Lowestoft to Sheerness), see red and blue lines with stars. This is partly related to the larger storm surge in the southern North Sea, and partly related to the smaller tidal ranges and MHWS at the southern stations (being closer to the tidal amphidrome), where the MHWS can be exceeded for a long duration with slowing moving storms. The larger time integrated excess elevations in the half-speed experiment (representing the 1953 storm) compared with the actual-speed experiment (representing the 2013 storm) suggests that, despite the smaller peak water level, the longer positive surge duration associated with slower SPS was likely an important natural factor leading to the larger flooding in 1953.

Results in this section were based on the FVCOM model simulations from 4 December 17:00 to 8 December 21:00 in 2013. Simulations after that period were not included because strong winds from another storm on 13-20 December 2013 resulted in strong tide-surge interactions on 8-12 December 2013 in the double-speed experiment, which were not covered in the actual- and half-speed experiments. However, since the new storm started to act on the UK east coast around 4 days after Xaver without resulting in water levels above MHWS except one instance at Lowestoft, it did not affect the Xaver surge in all experiments.

3.2 Influence of SPS on surge and tide-surge interaction

Water levels induced by surge-only (η_S, experiments $\mathrm{V} - \mathrm{VII}$) at different SPS are shown in Figure 5a. The magnitude and duration of η_S show a strong dependence on SPS. The surge remains positive for ~32 hours at actual SPS and as expected doubling the SPS result in a halved positive surge duration, and vice-versa (black and blue lines, Figure 5a). The peak surge continually increases southward for all SPS values (see Figure 5c, lines with circles), and shows a spatially variant response to SPS. At locations close to the storm track (Aberdeen), the peak surge decreases with decreasing SPS. At all other locations, however, the peak surge at actual speed is larger than that at double/half speed. It shows that the propagation speed of Xaver in 2013 was an important factor contributing to the stronger surge in the North Sea compared to the 1953 storm.

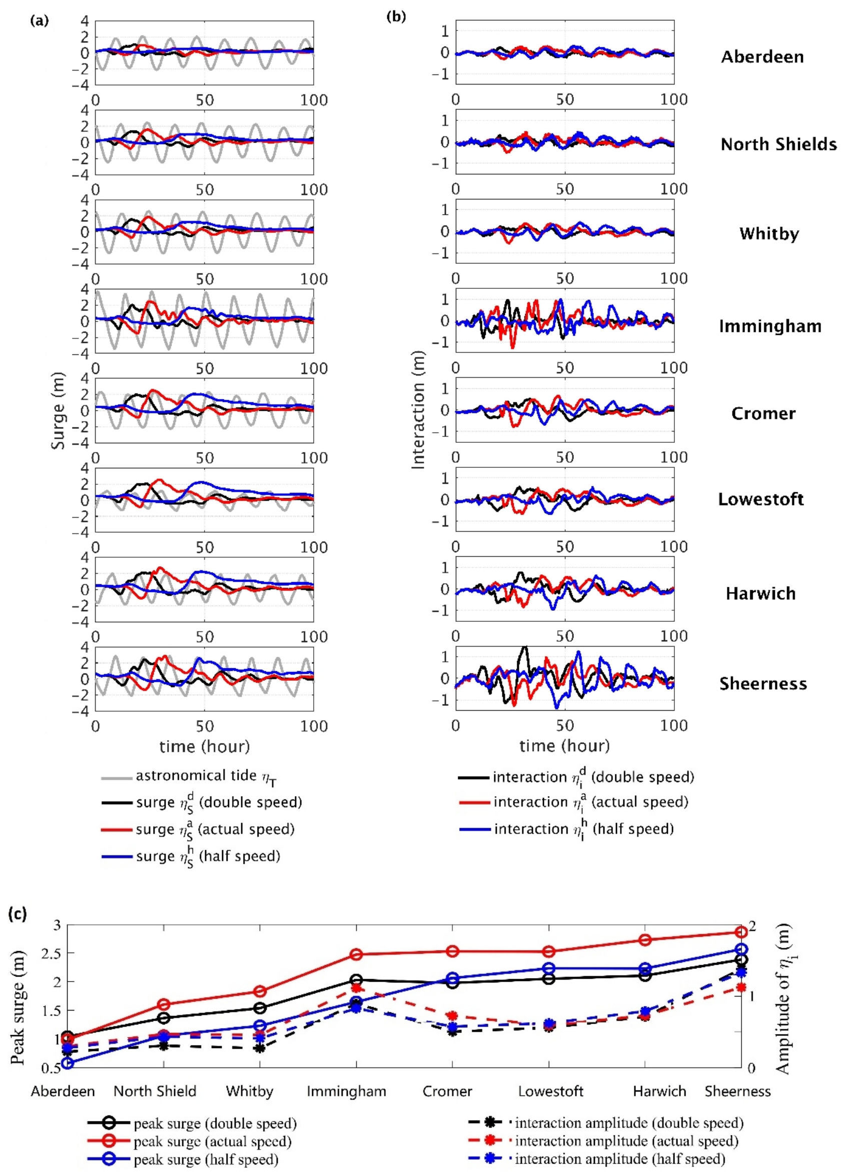

Figure 5. (a) Storm surge η_S, (b) water level due to tide-surge interaction ($\eta_i = \eta_{TS} - \eta_T - \eta_S$), and (c) peak surge (maximum η_S) and the interaction amplitude of η_i during the storm event. Here the amplitude of η_i is defined as half of the difference between the maximum and minimum values of η_i: $\left(\max(\eta_i) - \min(\eta_i)\right)/2$. Gray line shows the astronomical tide for guidance. Plots were based on the FVCOM model results from 4 December 17:00 to 8 December 21:00 in 2013.

The water level due to tide-surge interaction (η_i) for actual, doubled and halved SPS was calculated by subtracting the surge (η_S) and tidal elevation (η_T) from the total water level (η_{TS}),

$$\eta_i = \eta_{TS} - \eta_T - \eta_S. \quad (5)$$

Note that radiational (weather-related) tides are included in η_S but not in η_T so that double-counting of the radiational tidal component is not relevant here (Williams et al., 2018). For all SPS, tide-surge interaction results in an increase or decrease in η_i which keeps fluctuating throughout the storm event, with η_i more sensitive to SPS along the southern coast than the northern coast (Figure 5b). To quantify the maximum strength of the tide-surge interaction during the storm, the amplitude of η_i, defined as half of the difference between the maximum and minimum values of η_i, $\left(\max(\eta_i) - \min(\eta_i)\right)/2$, was calculated for all stations and is shown in Figure 5c (see lines with asterisks). For all SPS, the amplitude of η_i first increases from Aberdeen to Immingham, decreases towards Lowestoft, then increases again towards Sheerness. The largest amplitude of η_i occurs at Immingham and Sheerness where the tidal ranges are the largest. This spatially varying pattern matches well with the along-coast variation of the tidal range, which peaks near Immingham and drops to its minimum near Lowestoft. Doubling and halving SPS both result in larger amplitudes of tide-surge interaction at the three southernmost stations (Lowestoft, Harwich, and Sheerness), while the duration of large η_i is decreased and increased, respectively (see black and blue lines in Figure 5b). The largest interaction amplitude η_i occurred at actual speed from Aberdeen to Cromer, however, η_i at actual speed is smaller than that at double and half speed at Sheerness. This is due to the peak surge at actual speed occurring close to high water in the northern stations, but occurred on rising tides at Harwich and Sheerness.

The standard deviation of η_i for each SPS was also calculated to quantify the overall influence of SPS on the fluctuations of water level due to tide-surge interaction throughout the storm event,

$$\sigma = \left[\frac{\sum_{i=1}^{N}(\eta_i - \acute{\eta}_i)^2}{N-1}\right]^{1/2}. \quad (6)$$

Here $\acute{\eta}_i$ and N are respectively the time average and number of time steps in the η_i time series from 4 December 17:00 to 8 December 21:00. Spatial distributions of σ for each SPS are shown in Figure 6. For all SPS, σ is much smaller in the northern North Sea than that in the south. The SPS impact on σ is site specific, depending on its impact on η_S and the phase difference between η_S and η_T. Since η_S at actual speed is larger than that at doubled/halved speed in most areas, the interaction at actual speed is stronger than other SPS if the peak surge tends to occur near high water (e.g., from Aberdeen to Lowestoft, see Figure 5a). At locations where the peak surge happens to arrive at rising tide near high water at actual SPS (e.g., Harwich and Sheerness), the interaction is stronger at half and double SPS, in which cases η_S is only slightly smaller but the peak surge arrives near high water.

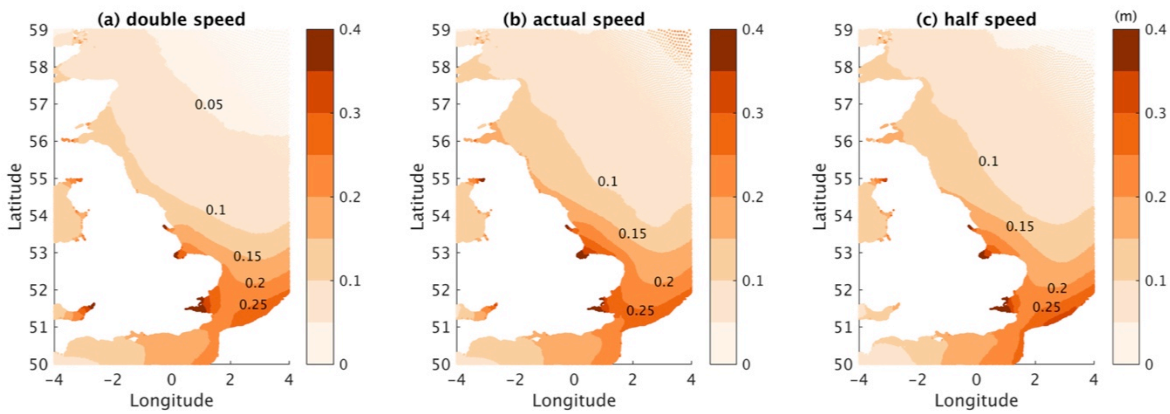

Figure 6. Standard deviation of surface elevation ($\eta_{i.}$) due to tide-surge interaction for doubled, actual, and halved SPS.

3.3 Influence of SPS on tides

Another way to consider the surge is as a modifier to the tide. The impact of surge on tides was investigated by fitting harmonic tidal constituents to the astronomical tide and tide affected by interaction ($\eta_T^{'}$) at each model grid point. A least-squares fit was used following the approach of Cartwright & Tayler (1971). Here, $\eta_T^{'}$ is calculated by subtracting the meteorological forcing induced water level η_S from the total water level η_{TS}, which also equals the astronomical tide plus the elevation resulted from tide-surge interaction:

$$\eta_T^{'} = \eta_{TS} - \eta_S = \eta_T + \eta_{i.}. \quad (7)$$

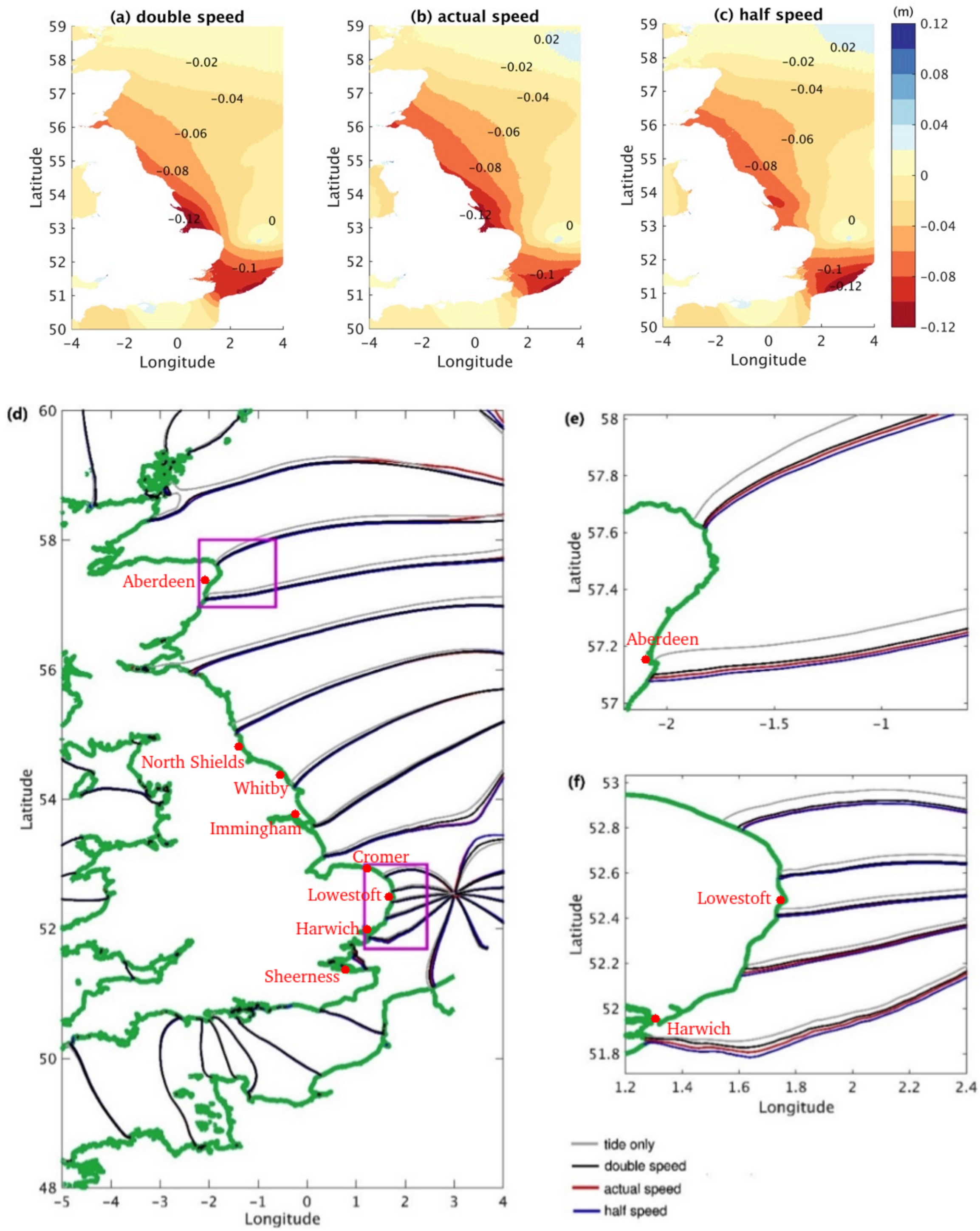

Figure 7. Changes in the amplitude (a-c) and phase (d-f) of the M2 tidal constituent due to tide-surge interaction, $\eta_T^{'}$. Negative values in (a-c) mean the M2 tidal amplitude affected by surge is smaller than the astronomical M2, and vice versa. Phase lines in (d-e) are plotted every 30 degrees (equivalent to ~1 hour).

Then, the impact of surge on the tide is quantified by the difference between the fitted tidal constituents of $\eta_T^{'}$ and those of the astronomical tide η_T, based on the FVCOM model results from 4 December 17:00 to 12 December 2013 17:00. In order to capture the impact of the storm using only 8 days of data, only the 4 main constituents M2, S2, O1, K1 were fitted. Since the tide is mostly dominated by the M2 constituent in the North Sea, only the changes in the M2 tidal constituent are discussed.

For all SPS, the average phase of M2 over the 8 days is advanced by around 5 degrees, indicating the M2 fitted to $\eta_T^{'}$ rises an average of around 10 minutes earlier than M2 on η_T (Figure 7). The phase change increases everywhere with storm duration from double speed to half speed. The averaged changes in the tidal phase due to tide-surge interaction at the UK east coast are relatively small compared to the results of Horsburgh & Wilson (2007), which were based on historical data analysis. This may be related to the storm lasting shorter than the fitted 8-day period, hence the tide remains unaffected by surge for some of this period.

Near the UK east coast, the magnitude of M2 is reduced by up to around 0.12 m due to the storm effects (Figures 7a-c). This is related to the temporary phase shift, which effectively reduces the power fitted to M2 over the 8 days. The influence of SPS on the magnitude of the change in the M2 tide amplitude is spatially variant and may be related to the arrival time of the maximum η_S with respect to the tide, as suggested by Prandle & Wolf (1978) and Kim et al. (2008).

Maps of peak surge η_S and skew surge for all SPS are shown in Figure 8. Skew surge is by definition less than η_S, and particularly at locations with large tidal ranges, the skew surge is also related to the arrival time of the peak surge with respect to η_T. As a result, the largest skew surge is found at locations in the southern North Sea with both large peak surge and small tidal ranges for all SPS. This largely explains why although the largest peak surge of the North Sea occurred near Sheerness during storm Xaver, the largest flood hazard occurred near Lowestoft (as shown in Figure 4b). The greater flood hazard at Lowestoft is a result of the peak surge occurring only 1 hr before high water and the water level remaining high at high tide due to weak tide-surge interaction; while at Sheerness, the peak surge occurred 2 hrs before high tide (see Figure 8h) and the water level dropped significantly at high tide due to strong interaction.

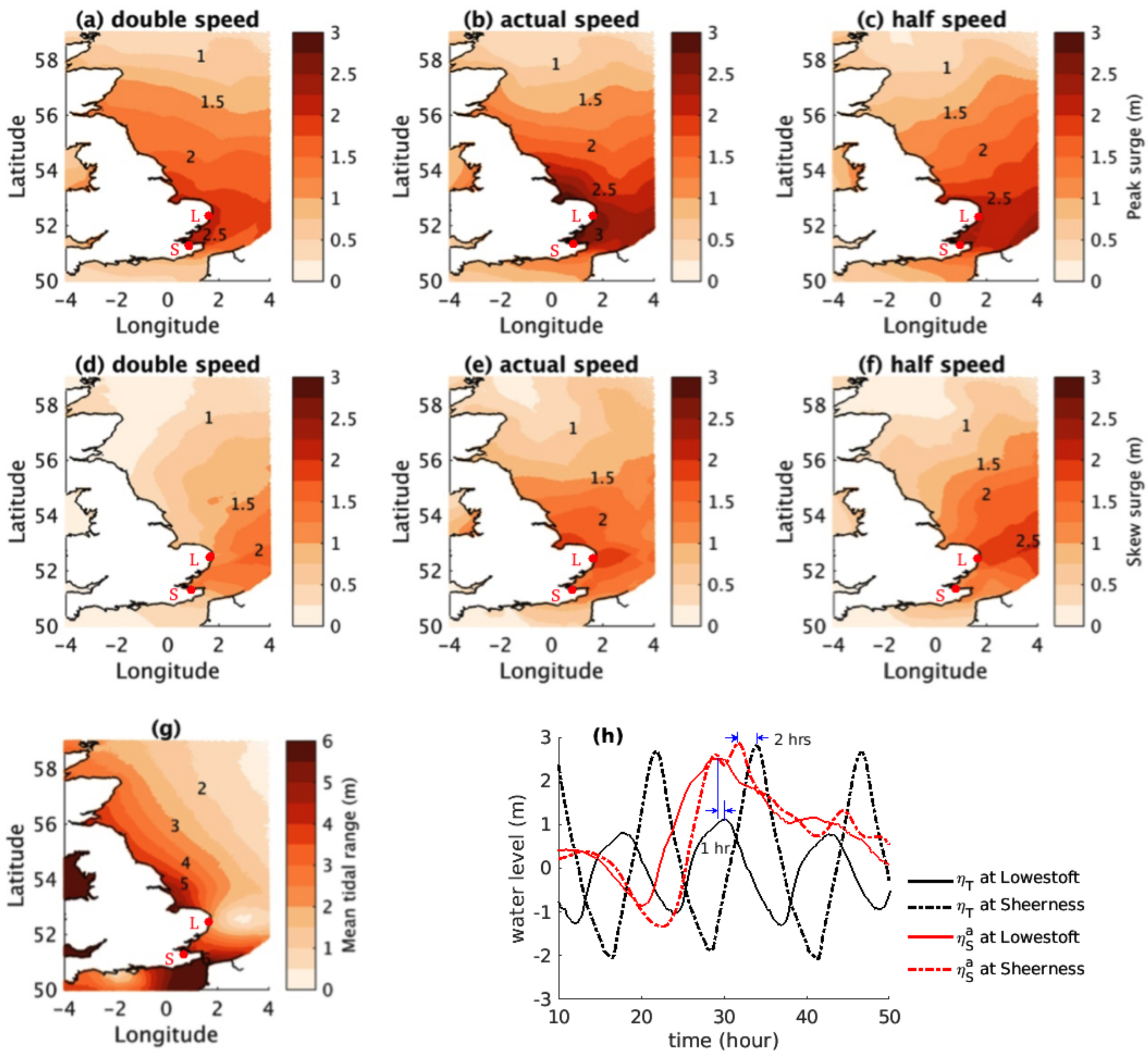

Figure 8. Distributions of the peak surge (a-c), skew surge (d-f) and mean tidal range (g) in the North Sea adjacent to the UK. The peak surge is the maximum η_S. The skew surge is defined as the difference between the maximum η_{TS} and the peak astronomical tidal elevation η_T during the storm. Different colour scales are used for (a-f) and (g) for clarity. L and S indicate gauge locations at Lowestoft and Harwich, respectively. (h) Tide/surge induced water levels at Lowestoft (solid lines) and Sheerness (dash-dotted lines), showing the arrival time of the peak surge with respect to tides. Here, red lines show the storm surge and black lines show the astronomical tides.

4 Physical mechanisms

4.1 Relative importance of wind and atmospheric pressure

The relative importance of atmospheric pressure gradients and wind forcing to water levels induced by offshore storm surge was investigated by calculating the changes in total water levels in experiments VIII and IX compared to those in experiment I. By setting the atmospheric pressure gradients to zero, the changes in total water level were less than 0.8 m during all stages of the tide at all stations. However, excluding the wind stress results in significant changes in water levels (up to 3 m, see Figure 9). This reveals that the storm surge along the UK east coast during Xaver is predominantly driven by wind set-up, while the atmospheric pressure gradients played a relatively small role. The dominant role of wind set-up in storm surges has also been found in other shallow seas such as the Seto Inland Sea (Kohno et al., 2007) and the eastern Irish Sea (Maskell, 2011).

4.2 Impacts of water depth and fetch length

Following the dominance of wind set-up on surge residuals, the semi-analytical surge model takes the wind to be the only external forcing and ignores tide-surge interaction. Hence, the surge is approximated by the wind set-up only. By assuming a time-periodic wind stress and surge response without any spatial differences in phase, the wind duration is equal to the surge period in the semi-analytical model, which is directly related to the time duration of the storm acting on the basin. The faster the storm travels across the basin (large SPS), the smaller the wind duration and surge period (small T). Ignoring the complex geometry and lateral bathymetry features, the semi-analytical model considers a rectangular-shaped, semi-enclosed basin to represent the North Sea.

For negligible bottom friction, Coriolis effect, constant water depth, and large wave length (small γ, e.g., with $T \geq 30$ hours), the locally generated surge due to wind set-up (second term of equation (2)) reduces to

$$\eta_{Sw} \approx \frac{\tau_{wx}}{\rho g H} x \sin(\omega t). \tag{8}$$

Equation (8) indicates the surge is approximately linear to the fetch length (i.e., the distance from the northern boundary) and inversely proportional to the water depth, as reported by Happer &

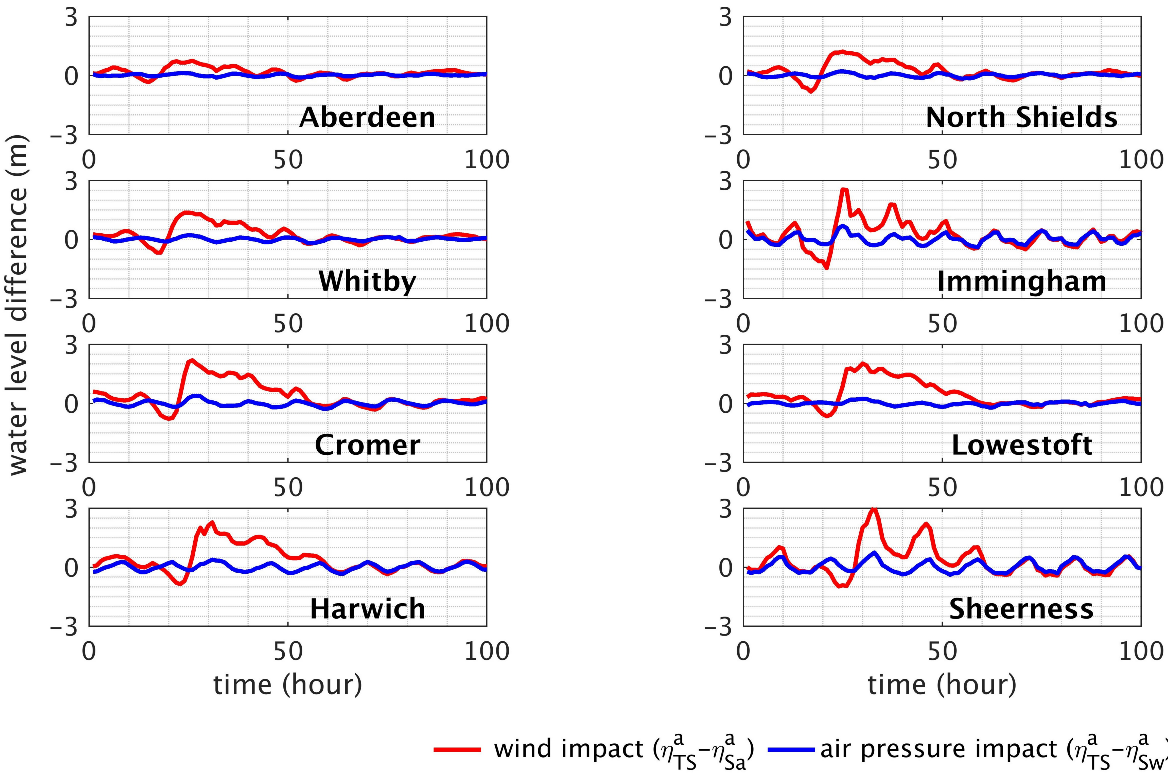

Figure 9. Changes in water levels due to air pressure impact (blue) and wind impact (red). Here the impact of air pressure and wind are measured by water level differences between experiment I, where both wind stress and air pressure gradients are included, and experiments VIII-IX, where air pressure gradients and wind stress are prescribed to be zero, respectively.

Sobey (1983) and Resio & Westerink (2008). Hence, decreasing the fetch and increasing water depth will result in a reduced surge. This helps explain the generally smaller peak surge in the deeper northern North Sea (shorter fetch) as compared with the shallower south (longer fetch), see Figures 8a-c. Note that equation (8) was derived by ignoring the water depth variations caused by tide and surge. In reality, the increase of water depth at high tide can result in a reduced maximum surge residual when the peak surge tends to occur near high water. This is another reason for the skew surge being smaller than the peak surge as shown in Figure 8. It can also be deduced that the tidal impact on storm surge increases with increasing tidal range for a given bathymetry. The inverse proportionality of surge to water depth also suggests that surge in shallow waters is more sensitive to tide-related depth variations than in deep waters. As a result, the strongest tide-surge interaction tends to occur in shallow regions with large tidal ranges as shown in Figure 6 (see also Kim et al., 2008).

The sensitivity of surge to water depth and fetch length is important to coastal flood hazard assessment. It suggests that coastlines fronted by shallower waters are more likely to have large flooding due to the stronger storm surge. The northeast coast of the UK (e.g., between Aberdeen and Immingham) is fronted by relatively deep waters and has a short(er) fetch length, thus the coastal flood hazard associated with the storm surge is small. The southeast coast is fronted by relatively shallow water with a long(er) fetch, where the tidal range is highly variable. At locations with small tidal ranges and MHWS (e.g., Lowestoft), the surge is large while the tide-surge interaction is weak, hence the arrival time of peak surge is hardly affected by tides. In this case, peak surge can coincide with high water depending on the arrival time of the storm, resulting in a high coastal flood hazard with a large skew surge. Lowestoft has a tidal range of 1.89 m and MHWS of 1.08 m. During Xaver, the peak surge coincided with high water at this location, resulting in a skew surge of up to 1.96 m and a time integrated excess elevation of 4.53×10^4 m·s at half SPS. At locations with large tidal ranges and MHWS (e.g., Sheerness), the tide-surge interaction is strong. The SPS strongly affects the arrival time of maximum surge residual, which tends not to occur near high water. The tidal range and MHWS at Sheerness are respectively 4.33 m and 2.96 m, where strong tide-surge interactions were generated during Xaver. This resulted in a smaller skew surge (1.45 m) and time integrated excess elevation (0.98×10^4 m·s) at half SPS as compared to Lowestoft (Figure 4c). These results suggest that effects of SPS, offshore bathymetry, and tidal range all combine to maximize potential flooding for slowly propagating storms in regions with broad shallow offshore bathymetry and small tidal ranges.

4.3 Sensitivity to wind duration: resonance effect

In this section, the idealized, semi-analytical surge model was used to systematically investigate the sensitivity of the storm surge to SPS, and to examine the possible resonance generation in the North Sea during Xaver. The SPS during Xaver ranges from 10 to 20 m/s, smaller than the long wave phase speed ($\sqrt{gH}$~30 m/s, with $H \sim 100$ m) in the northern North Sea where the storm centre passed, hence no Proudman resonance was generated. Therefore, only the influence of SPS on possible shelf resonance due to the associated wind period will be discussed.

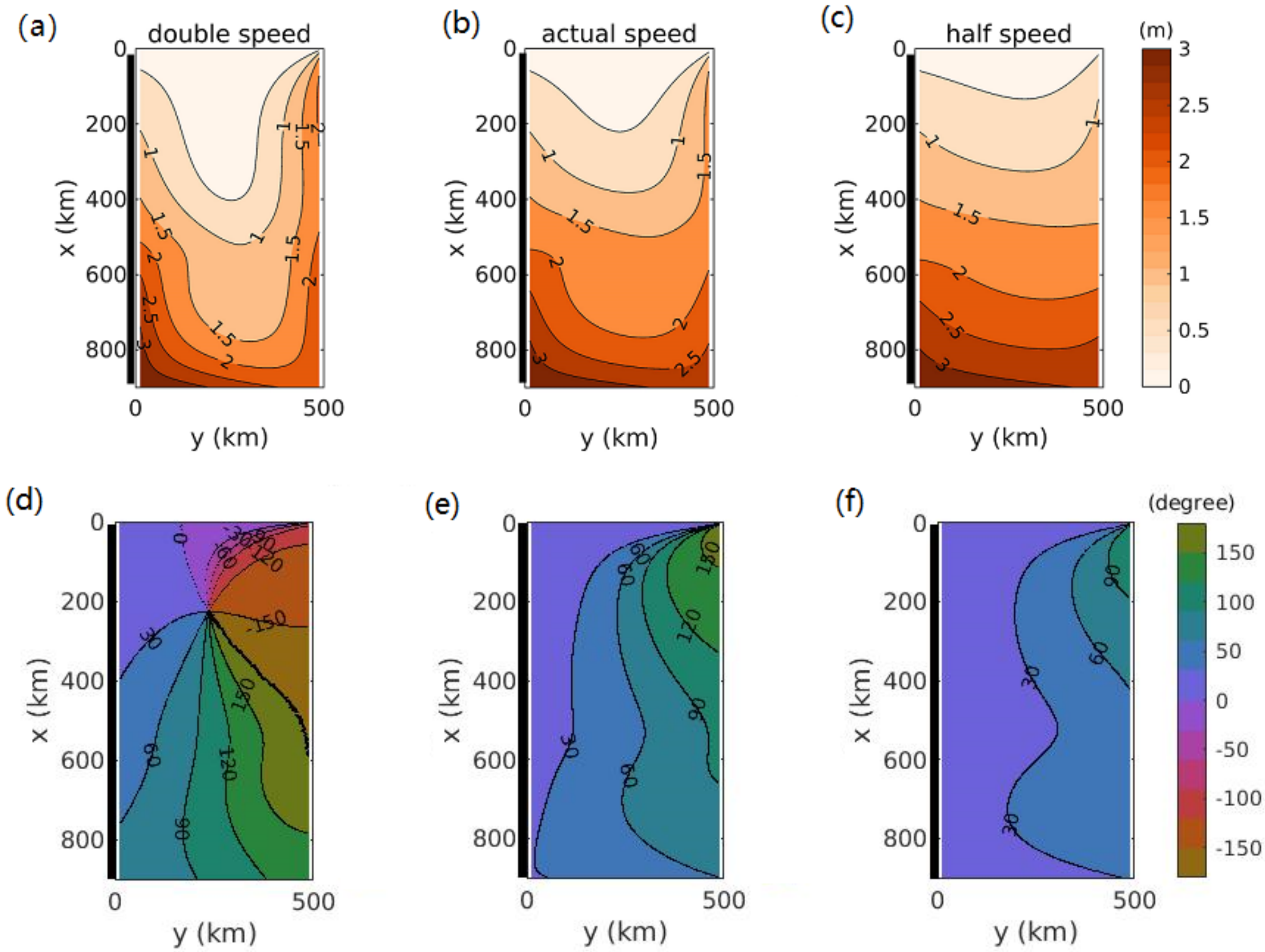

Figure 10. Spatial distributions of the (a-c) surge amplitude and (d-f) phase for double, actual, and half SPS. The thick black line indicates the location of the UK east coast.

To qualitatively represent the bathymetric variations in the North Sea, the semi-analytical model now considers a tangent-hyperbolic depth profile (Figure 1b). It also considers a time-periodic wind stress with its amplitude linearly decreasing along the UK east coast so that the spatial variations of the wind field during Xaver are qualitatively included (see equation (4) and Figure 2). The FVCOM experiments with double, actual and half speed of Xaver are approximately represented with a positive wind duration of 16, 32 and 64 hours.

The amplitude and phase of the surge for each SPS are shown in Figures 10a-c and Figures 10d-f, respectively. The semi-analytical model qualitatively reproduces the surge behaviors in the North Sea for each SPS as obtained from the FVCOM model results (comparing Figures 10 a-c with Figures 8 a-c). For all SPS, the surge amplitude is larger in the shallower south than in the deeper north, and it peaks along the UK east coast (the right-hand side of the storm track) due to Coriolis effect (Figures 10a-c). The surge phase increases along the coast in a counter-clockwise direction (Figures 10d-f), behaving like a forced coastal trapped wave (Clarke 1977). The cross-basin differences in the surge amplitude and phase decrease significantly with decreasing SPS. For double speed, the surge amplitude/phase decreases/increases significantly along the coast with almost no surge responses in the centre of the northern North Sea (see Figure 10a, 10d). The coastal trapped wave feature becomes less evident with increasing wind duration (decreasing SPS). The surge is almost laterally uniform for half speed (see Figure 10c, 10f), suggesting the surge is then dominated by along-basin dynamics with limited cross-basin responses. It implies the Coriolis effect on the North Sea surge, which is considered in the semi-analytical model setup here, is small for small SPS. The consistency between the FVCOM model and semi-analytical model indicates the simplified geometry, bathymetry and boundary conditions used in the semi-analytical model are appropriate, and the dominant processes governing the storm surge are reasonably resolved. The surge amplitude is slightly over-predicted at the southwest part of the North Sea by the semi-analytical model and under-predicted at the southeast part. These discrepancies are probably caused by the strong tidal currents in the English Channel and the shallow bathymetry of the German Bight, which are not considered in the semi-analytical model due to the simplified bathymetry and geometry.

The low computational cost of the semi-analytical method allows a systematic investigation of the sensitivity of surge to the SPS, which is translated into the positive wind duration $T/2$. Figure 11a shows the distributions of the surge amplitude along the UK east coast for $T/2$ varying from 5 to 100 hours. The surge amplitude is highly sensitive to wind durations for $T/2$ between 5 and 35 hours, and it becomes less dependent on the wind duration for $T/2$ >50 hours. Two resonance peaks are found for $T/2$ <35 hours (Figure 11a). The largest surge amplitude (~4 m) occurs at $T/2$ =7.5 hours, which is associated with a resonance frequency of 1.16×10^{-4} rad/s, close to the inertial frequency *f* for the North Sea. This resonance frequency is smaller than the reference frequency ($\omega_{ref} = \frac{2\pi\sqrt{gH_{av}}}{L} = 1.65\times10^{-4}$ rad/s, $T/2 = 5.29$ hours, with H_{av} the mean water depth of the basin), at which Chen et al. (2016) found as the first resonance for a rectangular basin with a uniform depth and an aspect ratio of 0.5 (approximates the North Sea). The second

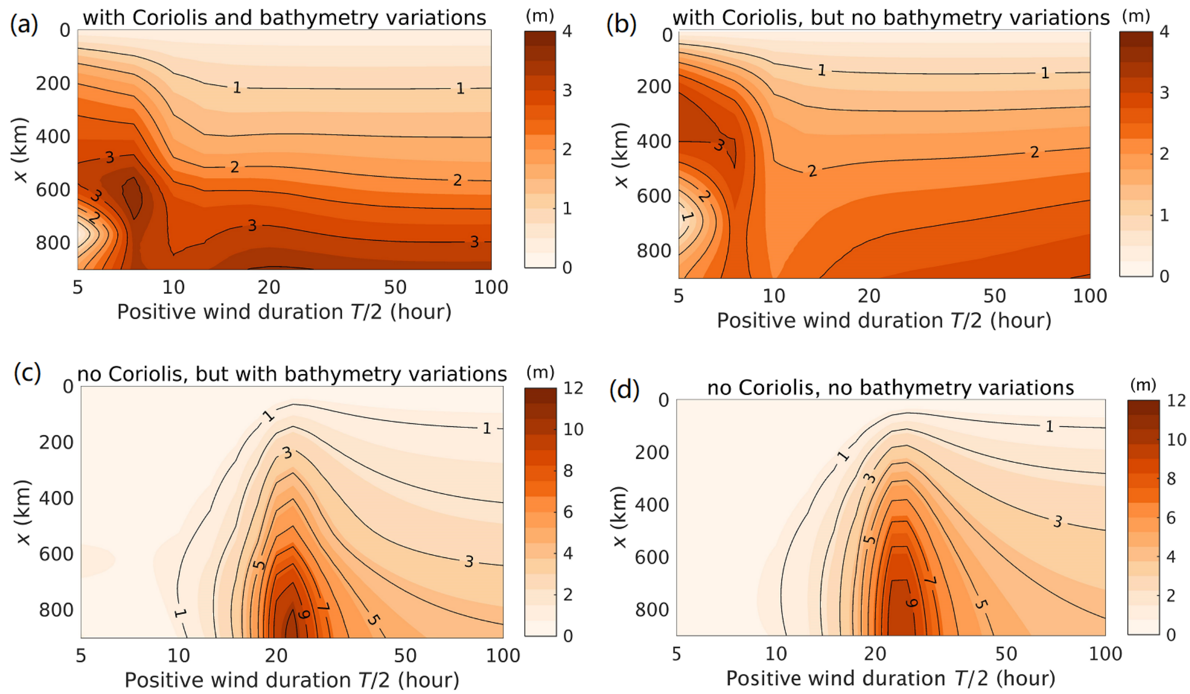

Figure 11. (a) Sensitivity of the surge amplitude along the UK east coast to positive wind duration $T/2$, considering both bathymetry variations and Coriolis effect, $f = 1.18 \times 10^{-4}$ rad/s. (b) Same results but using the mean water depth with Coriolis effect, $f = 1.18 \times 10^{-4}$ rad/s. (c) Same results considering the bathymetry variations but no Coriolis effect. (d) Same results but using the mean water depth without Coriolis effect. Here, a logarithmic scale was used for the horizontal axis, and different colour scales were used for (a) and (b) compared to those for (c) and (d) for clarity.

resonance occurs at $T/2 = 20$ hours (surge amplitude ~3.5 m) and is associated with a resonance frequency of 4.36×10^{-5} rad/s. The actual positive wind duration of Xaver (32 hours), was close to this resonance wind duration and therefore likely to have contributed greatly to the occurrence of the strongest North Sea storm surge over the past 60 years. For most SPS, the surge amplitude is smaller at the deeper northeast coast than the shallower southeast coast, consistent with the FVCOM results. Note that the wind stress during a real storm event contains a wide variety of frequencies (see Chen et al., 2015). The sensitivity study here considers only one wind frequency in order to show the surge response to each wind frequency. To reproduce more realistic wind-generated surge responses, more wind frequencies could be considered in the semi-analytical model.

To understand the role of the geometry, topography, and Coriolis effects in generating resonance in the North Sea, the sensitivity of the surge amplitude to positive wind duration were investigated by conducting another three semi-analytical experiments where the bathymetry variations and/or the Coriolis effect were excluded. Figures 11b-d show the sensitivity of surge amplitude along the UK east coast to the positive wind duration $T/2$ when excluding only the bathymetry variations by using a mean water depth (Figure 11b), excluding only the Coriolis effect (Figure 11c), and excluding both bathymetry variations and Coriolis effect (Figure 11d). When considering a constant water depth with Coriolis effect, resonance occurs at $T/2$ =5 hours near the reference frequency (at $T/2 = 5.29$ hours) as found by Chen et al. (2016), see Figure 11b. It suggests the different resonance frequencies between Figure 11a and Chen et al (2016) are related to the along-coast bathymetric variations in the North Sea. Comparing Figure 11b with 11a, it is found that the resonance near the reference frequency is only slightly affected by bathymetry variations; however, the second resonance is significantly changed, with the surge amplitude constantly increasing with increasing T for constant water depths. When excluding Coriolis effects (still with bathymetry variations), only one resonance occurs at $T/2 = 22.5$ hours (see Figure 11c). Resonance occurs at $T/2 = 25$ hours when using a constant mean water depth with no Coriolis effect (see Figure 11d). It suggests that the second resonance observed in Figure 11a is associated with the dimensions of the North Sea, i.e., its length and mean water depth. In general, including Coriolis effect leads to a weaker resonance (see different colour scales between Figure 11a,b and Figure 11c,d), due to cross-basin surge responses. The surge amplitude for large wind durations is only slightly changed, confirming the Coriolis effect on the surge is small for slow SPS. These results suggest the two resonances observed in Figure 11a result from the combined effects of the dimensions and bathymetry of the North Sea, and the Coriolis effect.

The tide-surge interaction, despite its potential significance to coastal floods, was not included in the semi-analytical model. The impact of SPS on tide-surge interaction and its sensitivity to the arriving time of the surge with respect to tide could be systematically investigated in future work by using a semi-analytical model which resolves tide, surge and their interaction, as considered by Prandle & Wolf (1978).

5 Conclusions

Storm propagation speed (SPS) strongly impacts coastal flood hazards due to extreme water levels. This study focused on the influence of SPS on coastal flood hazard caused by offshore storms and their physical mechanisms. As a case study, the SPS impact on the UK east coast, where storms frequently cause coastal floods without making landfalls, was investigated using a shelf sea model based on FVCOM. The storm Xaver, which caused the largest North Sea surge over the past 60 years, was studied as a base scenario. Another eight experiments were designed to quantitatively evaluate the SPS impact on coastal flood potentials, storm surge, tide-surge interaction and the relative importance of wind and atmospheric pressure. The actual speed of Xaver was halved or doubled in these experiments to evaluate the influence of SPS. The half-speed experiment qualitatively represents the 1953 storm, which caused the devastating coastal floods along the UK east coast. Results show the largest skew surge occurs at the actual speed and the largest time integrated excess elevation at half speed. This implies that the slow SPS of the 1953 storm was an important natural contributor to the devastating flood hazard.

The SPS impacts the coastal flood hazard through influencing the storm surge, tide-surge interaction and its impact on tides. The largest surge occurs when the storm travels at actual speed, while doubling/halving the SPS results in a smaller surge and a shorter/longer surge duration. For all SPS, the tide-surge interaction is stronger in the northern North Sea than the south. By doubling or halving the SPS, fluctuations of the water level due to tide-surge interactions are enhanced near Sheerness, where the tide-surge interaction is the strongest along the UK east coast. Tides in the North Sea are generally modified by surge due to the tide-surge interaction. The amplitude of the M2 tide, which is the dominant tidal constituent in the North Sea, is reduced by surge along the coast for all SPS. The magnitude of the surge-induced change in the M2 amplitude is spatially variable, and differs significantly with SPS. The averaged phase of the M2 tide over the storm is advanced by around 10 minutes for all SPS, with the change increasing by a further 4 to 10 minutes with SPS from double speed to half speed. The modified tide contributes to a skew surge smaller than peak surge everywhere in the North Sea, and the largest skew surge occurs at locations with large peak surge and small tidal range for all SPS (e.g., Lowestoft).

Wind was the predominant meteorological forcing in the North Sea throughout Xaver. An idealized, semi-analytical model was used to systematically investigate the physical mechanisms behind the impact of SPS. The model only includes the wind forcing, hence the wind duration is directly translated into the SPS. Considering a semi-enclosed rectangular basin with along-coast depth variations representative of the North Sea, the semi-analytical model qualitatively reproduces the surge behavior with respect to both spatial variability and dependence on SPS. Results indicate that the complex North Sea surge dynamics induced by offshore storms are primarily associated with the wind set-up, and that the main processes are reasonably resolved. Two resonances are found: the largest resonance near the inertial frequency and the second at positive wind duration of 20 hours. The second resonance period is close to the wind period during Xaver, suggesting that the wind forcing of Xaver may have contributed greatly to the occurrence of the largest North Sea surge over the past 60 years due to resonance. The resonance patterns are influenced by the dimensions and bathymetry of the North Sea, and Coriolis.

The sensitivity of surge to water depth and SPS is important to coastal flood hazard assessment. Coasts fronted by shallower waters are more likely to have large flooding due to the stronger storm surge. For coasts fronted by shallow waters with small tidal ranges (e.g., Lowestoft), the surge is large, and peak surge can coincide with high water depending on the arrival time of the storm, resulting in a high coastal flood hazard. Around shallow waters with large tidal ranges (e.g., Immingham and Sheerness), however, the tide-surge interaction is strong. Hence, the SPS can strongly influence the arrival time of the maximum surge residual, which tends not to occur near high water, resulting in a smaller potential flood hazard. Since the duration of high surge increases with decreasing SPS, it can be deduced that slowly propagating offshore storms are likely to cause significant flooding in shallow regions with small tidal ranges.

Acknowledgments and Data

This work is funded by the NERC BLUEcoast project (NE/N015894/1). We appreciate the tide gauge data support by the British Oceanography Data Centre, tide and meteorological forcing data from the Marine Data Products team at National Oceanography Centre (NOC), support from Michela De Dominicis and Judith Wolf on using the Scottish Shelf Sea Model. We appreciate the valuable comments from 5 reviewers, which have considerably helped to improve our paper. The model output of this study is available online at https://zenodo.org/record/1211505#.WsOG0K2E37h).

References

Azam, M. H., Samad, M. A., & Mahboob-Ul-Kabir. (2004). Effect of cyclone track and landfall angle on the magnitude of storm surges along the coast of Bangladesh in the northern Bay of Bengal. Coastal Engineering Journal, 46(03), 269-290.

Benavente, J., Del Río, L., Gracia, F. J., & Martínez-del-Pozo, J. A. (2006). Coastal flooding hazard related to storms and coastal evolution in Valdelagrana spit (Cadiz Bay Natural Park, SW Spain). Continental Shelf Research, 26(9), 1061-1076.

Bertin, X., Bruneau, N., Breilh, J.F., Fortunato, A. B., & Karpytchev, M. (2012). Importance of wave age and resonance in storm surges: The case Xynthia, Bay of Biscay. Ocean Modelling, 42, 16-30.

Brown, J. M., Souza, A. J., & Wolf, J. (2010). An investigation of recent decadal-scale storm events in the eastern Irish Sea. Journal of Geophysical Research: Oceans, 115(C5).

Brown, J. M., & Wolf, J. (2009). Coupled wave and surge modelling for the eastern Irish Sea and implications for model wind-stress. Continental Shelf Research, 29(10), 1329-1342.

Cavallo, E. A., & Noy, I. (2010). The Aftermath of Natural Disasters: Beyond Destruction, CESifo Forum, 11(2), 25-35.

Cartwright, D.E., Tayler, R.J. (1971). New computations of the tide-generating potential, Geophysical Journal International, 23(1), 45-73.

Charnock, H. (1955). Wind stress on a water surface. Quarterly Journal of the Royal Meteorological Society, 81(350), 639-640.

Chen, C., Liu, H., & Beardsley, R. C. (2003). An unstructured grid, finite-volume, three-dimensional, primitive equations ocean model: application to coastal ocean and estuaries. Journal of atmospheric and oceanic technology, 20(1), 159-186.

Chen, W. L., Roos, P. C., Schuttelaars, H. M., & Hulscher, S. J. (2015). Resonance properties of a closed rotating rectangular basin subject to space-and time-dependent wind forcing. Ocean dynamics, 65(3), 325-339.

Chen, W. L., Roos, P. C., Schuttelaars, H. M., Kumar, M., Zitman, T. J., & M. H. Hulscher, S. J. (2016). Response of large-scale coastal basins to wind forcing: influence of topography. Ocean Dynamics, 66(4), 549-565.

Choi, B.H., Kim, K.O., Yuk, J.H. & Lee, H.S. (2018). Simulation of the 1953 storm surge in the North Sea. Ocean Dynamics, 1-19.

Clark, A.J., (1977). Observational and numerical evidence for wind-forced coastal trapped long waves. Journal of Physical Oceanography, 231-247.

Davies, T., Cullen, M. J. P., Malcolm, A. J., Mawson, M. H., Staniforth, A., White, A. A., & Wood, N., (2005). A new dynamical core for the Met Office's global and regional modelling of the atmosphere, Quarterly Journal of the Royal Meteorological Society, 131, 1759-1782.Flather, R. A. (1994). A storm surge prediction model for the northern Bay of Bengal with application to the cyclone disaster in April 1991. Journal of Physical Oceanography, 24(1), 172-190.

Ganske, A., Fery, N., Gaslikova, L., Grabemann, I., Weisse, R. and Tinz, B. (2018). Identification of extreme storm surges with high-impact potential along the German North Sea coastline. Ocean Dynamics, 68(10), 1371-1382.

Garvine, R. W. (1985). A simple model of estuarine subtidal fluctuations forced by local and remote wind stress. Journal of Geophysical Research: Oceans, 90(C6), 11945-11948.

Haigh, I. D., Wadey, M. P., Wahl, T., Ozsoy, O., Nicholls, R. J., Brown, J. M., Horsburgh, K., & Gouldby, B. (2016). Spatial and temporal analysis of extreme sea level and storm surge events around the coastline of the UK. Scientific Data, 3, 160107.

Happer, B.A. & R.J. Sobey (1983), Open boundary conditions for open-coast Hurricane storm surge, Coastal Engineering, 7, 75-84.

Harwood, P. (2013). Highest North Sea Surge for 60 Years. eSurge. Available Online at: http://www.storm-surge.info/highest-north-sea-surge-60-years (Accessed Nov 22, 2017).

Horsburgh, K. J., & Wilson, C. (2007). Tide-surge interaction and its role in the distribution of surge residuals in the North Sea. Journal of Geophysical Research: Oceans, 112(C8).

Hussain, M. A., Tajima, Y., Hossain, M. A., & Das, P. (2017). Impact of Cyclone Track Features and Tidal Phase Shift upon Surge Characteristics in the Bay of Bengal along the Bangladesh Coast. Journal of Marine Science and Engineering, 5(4), 52.

Irish, J. L., Resio, D. T., & Ratcliff, J. J. (2008). The influence of storm size on hurricane surge. Journal of Physical Oceanography, 38(9), 2003-2013.

Jelesnianski, C. P. (1972). SPLASH (Special Program to List Amplitudes of Surges from Hurricanes): 1. Landfall storms, NOAA Tech. Memo. NWS TDL-46, 56 pp., NOAA, Silver Spring, Md.

Jonkman, S.N., & Kelman, I. (2005). An analysis of the causes and circumstances of flood disaster deaths. Disasters, 29(1), 75-97.

Kates, R. W., Colten, C. E., Laska, S., & Leatherman, S. P. (2006). Reconstruction of New Orleans after Hurricane Katrina: a research perspective. Proceedings of the national Academy of Sciences, 103(40), 14653-14660.

Kennedy, A.B., Gravois, U., Zachry, B.C., Westerink, J.J., Hope, M.E., Dietrich, J.C., Powell, M.D., Cox, A.T., Luettich Jr, R.A. and Dean, R.G., (2011). Origin of the Hurricane Ike forerunner surge. Geophysical Research Letters, 38(8).

Kim, S.Y., Yasuda, T., Mase, H. (2008). Numerical analysis of effects of tidal variations on storm surges and waves. Applied Ocean Research, 30, 311-322.

Kohno, N., Kamakura, K., Minematsu, H., Yorioka, Y., Hisashige, K., Shinizu, E., Sato, Y., et al. (2007). The mechanism of the storm surges in the Seto Inland Sea caused by Typhoon Chaba [0416]. Tech. Rev, 9.

Liu, Y., & Irish, J. L. (2019). Characterization and prediction of tropical cyclone forerunner surge. Coastal Engineering, 147, 34-42.

Lyddon, C., Brown, J. M., Leonardi, N., & Plater, A. J. (2018). Flood hazard assessment for a hyper-tidal estuary as a function of tide-surge-morphology interaction. Estuaries and coasts, 41(6), 1565-1586.

Maskell J. (2011). Modelling storm surge in the Irish and Celtic Sea using a finite element model (Telemac). Doctoral dissertation. University of Liverpool. Retrieved from the Brunswick Library Store, Liverpool, the UK.

Mei, W., Pasquero, C., & Primeau, F. (2012). The effect of translation speed upon the intensity of tropical cyclones over the tropical ocean. Geophysical Research Letters, 39(7).

Monserrat, S., Vilibic, I., Rabinovich, A. B. (2006). Meteotsunamis: atmospherically induced destructive ocean waves in the tsunami frequency band. Natural Hazards and Earth System Science, 6 (6), 1035-1051.

Olfateh, M., Callaghan, D. P., Nielsen, P., & Baldock, T. E. (2017). Tropical cyclone wind field asymmetry—Development and evaluation of a new parametric model. Journal of Geophysical Research: Oceans, 122(1), 458-469.

Peng, M., L. Xie, & Pietrafesa L. J. (2004). A numerical study of storm surge and inundation in the Croatan-Albemarle-Pamlico estuary system, Estuarine Coastal Shelf Sci., 59, 121– 137.

Peng, M., L. Xie, & Pietrafesa L. J. (2006). A numerical study on hurricane-induced storm surge and inundation in Charleston Harbor, South Carolina, J. Geophys. Res., 111, C08017, doi:10.1029/2004JC002755.

Prandle, D. and Wolf, J. (1978). The interaction of surge and tide in the North Sea and River Thames. Geophysical Journal International, 55(1), 203-216.

Proudman, J. (1929). The effects on the sea of changes in atmospheric pressure, Geophys. Suppl. Mon. Notices R. Astr. Soc., 2(4), 197-209.

Rego, J.L., & Li, C. (2009). On the importance of the forward speed of hurricanes in storm surge forecasting: A numerical study. Geophysical Research Letters, 36(7).

Risk Management Solutions (2003). 1953 U.K. floods: 50-year retrospective. Retrieved from https://forms2.rms.com/rs/729-DJX-565/images/fl_1953_uk_floods_50_retrospective.pdf

Rucińska, D. (2019). Describing Storm Xaver in disaster terms. International journal of disaster risk reduction, 34, 147-153.

Sibley A., Cox D., Titley H. (2015). Coastal flooding in England and Wales from Atlantic and North Sea storms during the 2013/2014 winter. Weather. 70 (2), 62-70.

Souza, A.J., Brown, J.M., Williams, J.J., & Lymbery, G. (2013). Application of an operational storm coastal impact forecasting system. Journal of Operational Oceanography, 6 (1). 23-26.

Staneva, J., Alari, V., Breivik, Ø., Bidlot, J.-R., Mogensen, K., 2017. Effects of wave-induced forcing on a circulation model of the North Sea. Ocean Dynamics, 67 (1), 81-101.

Swaden, D., Dunbar, I., Gilbert, S., Nicola, P., & Szönyi, M. (2014). After the storm: how the UK's flood defences performed during the surge following Xaver. Risk Nexus. Available online at: http://repo.floodalliance.net/jspui/handle/44111/2248

Tang, Y.M., Sanderson, B., Holland, G. and Grimshaw, R. (1996). A numerical study of storm surges and tides, with application to the North Queensland coast. Journal of Physical Oceanography, 26(12), 2700-2711.

Wadey, M. P., Haigh, I. D., Nicholls, R. J., Brown, J. M., Horsburgh, K., Carroll, B., Gallop, S., Mason, T. & Bradshaw, E. (2015). A comparison of the 31 January-1 February 1953 and 5-6 December 2013 coastal flood events around the UK. Frontiers in Marine Science, 2, 84.

Wei, X., Schramkowski, G.P. & Schuttelaars, H.M., (2016). Salt dynamics in well-mixed estuaries: Importance of advection by tides. Journal of Physical Oceanography, 46(5), 1457-1475.

Weisberg, R.H. and Zheng, L. (2006). Hurricane storm surge simulations for Tampa Bay. Estuaries and Coasts, 29(6), 899-913.

Williams, J., Irazoqui Apecechea, M., Saulter, A., & Horsburgh, K. J. (2018). Radiational tides: their double-counting in storm surge forecasts and contribution to the Highest Astronomical Tide. Ocean Science, 14(5), 1057-1068.

Willmott, C. J. (1981). On the validation of models. Physical geography, 2(2), 184-194.

Wolf, J. (1978). Interaction of tide and surge in a semi-infinite uniform channel, with application to surge propagation down the east coast of Britain. Applied Mathematical Modelling, 2(4), 245-253.

Wolf, J., Yates, N., Brereton, A., Buckland, H., Dominicis, M., Gallego, A., & O'Hara Murray, R. (2016). The Scottish Shelf Model. Part 1: Shelf-Wide Domain. Scottish Marine and Freshwater Science, 7(3), 151pp.

Zhang, C. (2012). Effect of hurricane forward speed and approach angle on coastal storm surge. Master thesis. Louisiana State University.

Zheng, X., Mayerle, R., Wang, Y., Zhang, H., 2018. Study of the wind drag coefficient during the storm Xaver in the German Bight using data assimilation. Dynamics of Atmospheres and Oceans 83, 64-74.

Appendix

Semi-analytical model description

In the idealized model, the surge forced by wind only is described by the linearized shallow water equations on the *f*-plane:

$$\frac{\partial u}{\partial x}+\frac{\partial v}{\partial y}+\frac{\partial w}{\partial z}=0; \tag{A.1}$$

$$\frac{\partial u}{\partial t}-fv=-g\frac{\partial \eta_{Sw}}{\partial x}+\frac{\partial}{\partial z}\left(A_v\frac{\partial u}{\partial z}\right). \tag{A.2}$$

$$\frac{\partial v}{\partial t}+fu=-g\frac{\partial \eta_{Sw}}{\partial y}+\frac{\partial}{\partial z}\left(A_v\frac{\partial v}{\partial z}\right). \tag{A.3}$$

Here *x* is the along-coast coordinate, positive directing towards the landward end; y is the lateral coordinate positive towards the east; *z* is the vertical coordinate, positive upward. The along-coast, lateral and vertical velocity components are denoted by $u,\ v$ and *w*, respectively. The wind-induced surge is denoted by η_{Sw}, and A_v is the vertical eddy viscosity assumed to be constant.

At the open boundary ($x=0$), η_{Sw} was prescribed as periodic function of time, i.e., $\eta_{Sw}=a_w\sin(\omega t)$. Here a_w is the surge amplitude at the northern entrance of the North Sea, $\omega=2\pi/T$ is the surge frequency (equals the wind frequency) and T the surge (wind duration) period, which can be directly related to the storm propagation speed. At the landward boundary ($x=L$, with *L* the basin length) and lateral boundaries ($y=0, B$, with *B* the basin width), the vertically integrated normal flux was required to vanish. At the bottom ($z=-H$), the normal velocity is required to vanish, $=-u\frac{\partial \mathrm{H}}{\partial x}-v\frac{\partial \mathrm{H}}{\partial y}$. A partial slip boundary condition was used to linearize the bottom friction, $A_v\,(\partial u/\partial z, \partial v/\partial z)=s(u,v)$ at $z=-H$, with s the partial slip parameter. At the free surface, the vertical velocity was determined by the time derivative of the surface elevation,

$$w=\frac{\partial \eta_{Sw}}{\partial t}. \tag{A.4}$$

The surface stress was directly related to the wind stress,

$$A_v\left(\frac{\partial u}{\partial z},\frac{\partial v}{\partial z}\right)=\frac{(\tau_{wx},\ \tau_{wy})}{\rho}. \tag{A.5}$$

Here ρ is the water density and the along-coast and lateral wind stress τ_{wx}, τ_{wy} were simplified as trigonometric functions of time t,

$$(\tau_{wx}, \tau_{wy}) = (\hat{\tau}_{wx}, \hat{\tau}_{wy})\sin(\omega t), \quad 0 \leq t \leq T, \qquad \text{(A.6)}$$

where $\hat{\tau}_{wx}$ and $\hat{\tau}_{wy}$ are respectively the amplitude of τ_{wx} and τ_{wy}. Equations (A.1)-(A.6) can be solved semi-analytically following Chen et al. (2016).

When assuming negligible Coriolis effect, lateral wind stress and bottom friction, the surge can be analytically solved for basins with a spatially uniform water depth and spatially uniform along-coast wind stress. In this case, the surge amplitude $\hat{\eta}_{Sw}$ can be described by a second-order ordinary differential equation:

$$T_1(x)\frac{d^2\hat{\eta}_{Sw}}{dx^2} + T_2(x)\hat{\eta}_{Sw} = F_{wind}(x), \qquad \text{(A.7)}$$

with $F_{wind}(x) = -\frac{\frac{d\hat{\tau}_{wx}}{dx}}{gH}$, $T_1(x) = H$, and $T_2(x) = \frac{\omega^2}{g}$. Equation (A.7) can be analytically solved together with the boundary conditions at $x = 0$ and $x = L$. The analytical solution reads

$$\eta_{Sw} = \left[\frac{a_w\cos(\gamma(x-L))}{\cos(\gamma L)} + \frac{\hat{\tau}_{wx}\sin(\gamma x)}{\rho g H\cos(\gamma L)}\right]\sin(\omega t), \text{with } \gamma = \frac{\omega}{\sqrt{gH}}\ . \qquad \text{(A.8)}$$

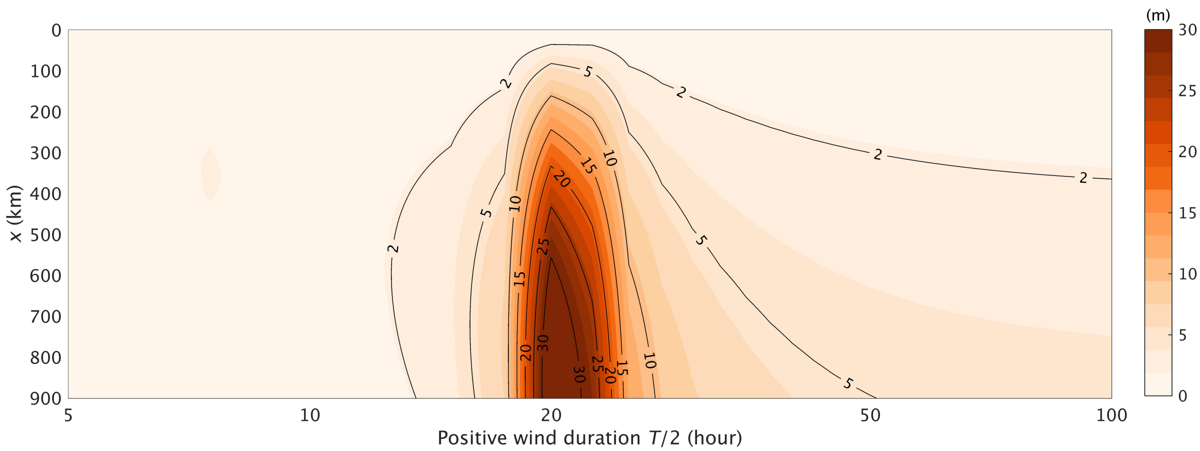

Figure A.1. Sensitivity of the surge amplitude along the UK east coast to positive wind duration T/2, for idealized frictionless basins with a spatially uniform bathymetry, wind stress, and no Coriolis. Same solutions were found using the analytical solution (2) and the semi-analytical model.

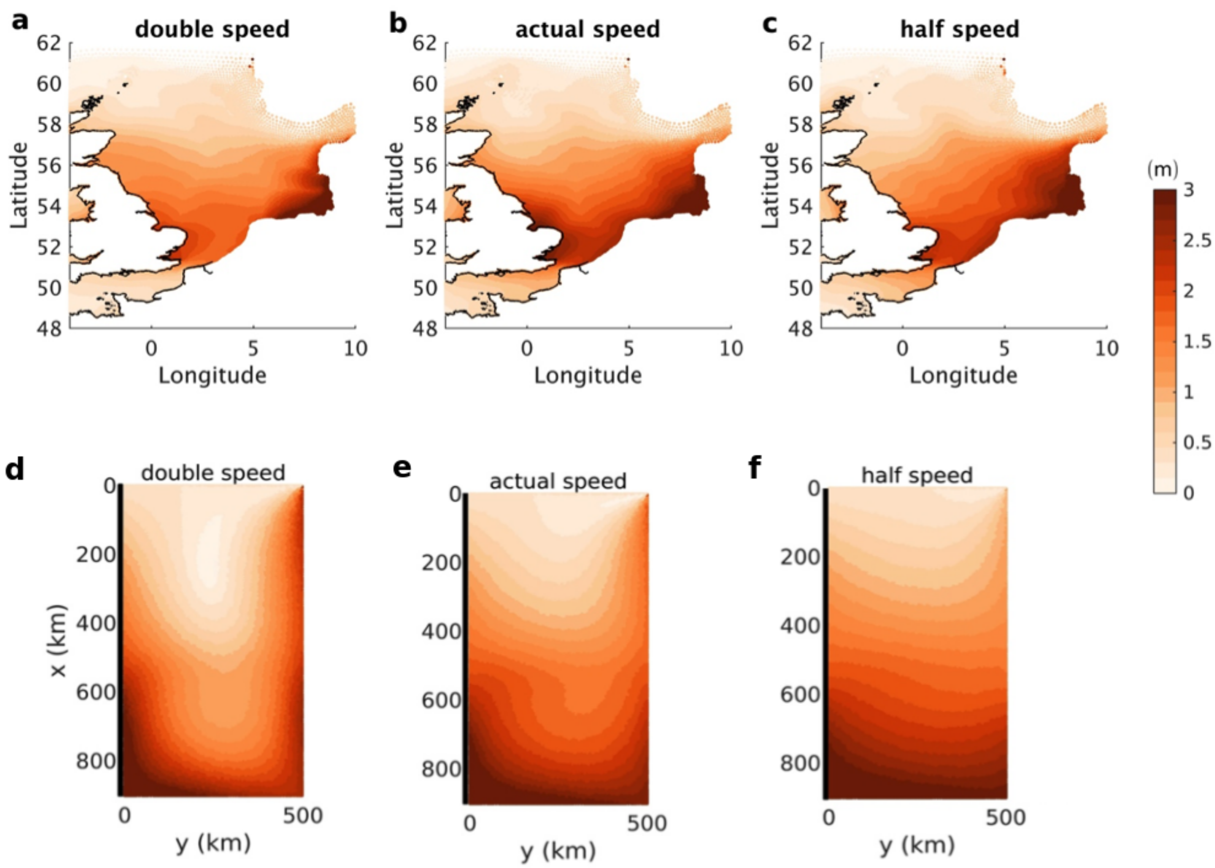

Figure A.2. Spatial distribution of peak surge for each SPS calculated from the FVCOM model (a-c) in comparison with that calculated from the semi-analytical model (d-f).

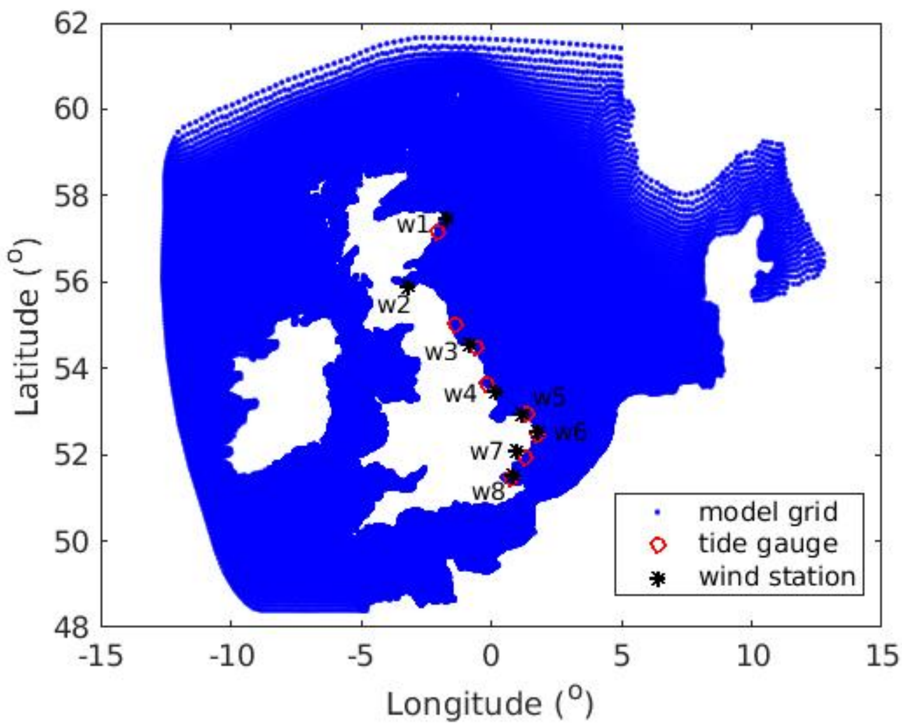

Figure **A.3.** Locations of wind stations near the 8 gauge stations along the UK east coast.

Table **A.1.** Mean error and root-mean-squared error for the wind forcing data near the UK east coast (from 4 December 17:00 to 8 December 21:00 in 2013).

Wind station	Mean error (m/s)	Root-mean-squared error (m/s)
w1	6.46	7.50
w2	4.76	5.83
w3	-2.77	4.84
w4	5.60	7.47
w5	2.44	5.27
w6	3.51	4.01
w7	2.96	3.58
w8	8.10	9.47
Average	3.88	6.00